1-1-2014

# Computational Investigation On The Structural Properties Of Neurofilaments And Their Sidearms

Lakshmi Jayanthi
*Wayne State University,*

**COMPUTATIONAL INVESTIGATION ON THE STRUCTURAL PROPERTIES OF NEUROFILAMENTS AND THEIR SIDEARMS**

by

**LAKSHMI JAYANTHI**

**DISSERTATION**

Submitted to the Graduate School

of Wayne State University,

Detroit, Michigan

in partial fulfillment of the requirements

for the degree of

**DOCTOR OF PHILOSOPHY**

2014

MAJOR: BIOMEDICAL ENGINEERING

Approved by:

_____

Advisor Date

_____

_____

_____

**DEDICATION**

*To*

*My parents and dear husband*

**ACKNOWLEDGEMENTS**

I am indebted to my advisor, Dr. Yeshitila Gebremichael, for all his encouragement and guidance through my doctoral study. I have been very fortunate to work with such a great mentor and extraordinary teacher. I owe my deepest gratitude to him for all his support and patience through my good and bad times.

I would like to thank my advisory committee members Dr. John Cavanaugh, Dr. Mahendra Kavdia and Dr. Michael Garcia for their helpful suggestions and support. I am also thankful to the Department of Biomedical Engineering for giving me this opportunity. I would also like to thank Dr. Paul Begeman for his support with the system. I am grateful to my colleague Dr. William Stevenson, for helping with setting up the simulations and for all his support. I would also like to thank my friends Dalia Alzebdah and Shruti for all their support and being such good friends.

I am greatly indebted to my family for all their love and support at every stage. Especially the encouragement of my in-laws and parents has been constant source of emotional support without which I wouldn't have come so far. I am very grateful to my brother-in-law Viswanath and sisters Hema and Manasa for encouraging me to excel in whatever I do. None of this would have been possible without the support of my loving husband Jaladhar, who is the guiding force and motivation behind every success I achieve.

**TABLE OF CONTENTS**

**LIST OF TABLES**

**LIST OF FIGURES**

**ABBREVIATIONS**

| | |
|---|---|
| ALS | Amyotropic lateral sclerosis |
| AFM | Atomic force microscope |
| EM | Electron Microscope |
| GBSW | Generalized Born with Smoothed Switching |
| IF | Intermediate filaments |
| MC | Monte Carlo |
| MD | Molecular Dynamics |
| MF | Microfilaments |
| MT | Microtubules |
| NCV | Nerve Conduction Velocity |
| NDD | Neurodegenerative disorders |
| NF | Neurofilaments |
| NFT | Neurofibrillary Tangles |
| PEB | Polyelectrolyte Brush |
| PD | Parkinson's Disease |
| PTM | Posttranslational Modification |
| QFDE | Quick Freeze Deep Etch |
| SCF | Self-Consistent Field theory |
| SPE | Spherical Polyelectrolyte Brush |

# Chapter I

## Background and Significance

Neurofilaments (NFs) are the most abundant axonal component of the large myelinated neurons, specific to central and peripheral nervous system. They have a key role in defining axonal physiology along with other cytoskeletal elements. Pathological accumulation of aggregated neurofilaments in the cell body of neurons is the hallmark of debilitating neurodegenerative disorders such as Parkinson's and Alzheimer's. Neurofilament compaction is also one of the pathological manifestations of traumatic axonal injury. However, the exact relation between the disorganized NFs and the etiology of the neurodegenerative disorders is yet to be fully understood. NFs are obligate heteropolymers assembled from three intermediate subunits NF light (L), Medium (M) and Heavy (H). The characteristic C-terminal domains (or sidearms) of these subunits have a predominant role in determining and maintaining axonal diameter. Further, they are also sites for extensive phosphorylation which is expected to play a key role in modulating their function. That said, the precise mechanism by which they regulate the axonal properties and the role of enzymatic phosphorylation-mediated regulation of their properties are yet to be understood. A descriptive understanding of the structural properties of C-terminal domains is expected to provide valuable insights into the function of NFs in health and disease.

### *Dissertation Outline*

The outline of this thesis is as follows: Chapter II gives an introduction to neurofilaments and their functional significance. In Chapter III, IV and V respective research problem is introduced, followed by relevant study design, results and conclusions. Future directions and concluding remarks are discussed in chapter VI.

# Chapter II

# Introduction

## *2.1. Intermediate Filaments*

The cytoskeleton of a eukaryotic cell is a network of interconnected structures of microtubules (MT), intermediate filaments (IF) and actin (or microfilaments) (MF) (Fuchs and Cleveland 1998; Herrmann and Aebi 2004), each characterized by unique structure, composition and functions. Being distinct in their biochemistry and physical features, IFs are described as polymorphic class of proteins different from MFs and MT. They are cell-specific proteins, expressed to maintain the cell's unique structural and mechanical properties (Fuchs and Cleveland 1998). They are classified into 5 types based on their structure, sequence characteristics and cell type specific expression. Type I and II represent keratins, and type III includes vimentin, desmin, peripherin, and glial fibrillary acidic protein. Neurofilaments (NFs) and nestin form type IV intermediate filaments. Type V consists of nuclear lamins (Herrmann and Aebi 2004). Table 2.1. shows the expression of IF in different vertebrate cells.

Table 2.1. Expression of IF proteins in different vertebrate cells
Source: (Steinert and Roop 1988)

| Type | IF Proteins | Origin |
|---|---|---|
| I &II | Acidic and neutral-basic Keratins | All epithelia |
| III | Vimentin | Mesenchymal Cells |
| III | Desmin | Myogenic Cells |
| III | Glial fibrillary acidic protein | Glial Cells and astrocytes |
| IV | Neurofilaments | Most Neurons |
| V | Lamins | Nuclear lamina of all eukaryotes |

*2.2. Neurofilaments*

Neurofilaments (NFs) are type IV intermediate filaments, most abundantly found in the large myelinated neurons of central (CNS) and peripheral nervous systems (PNS). For example in a giant squid axon, they constitute up to ~13% of the total protein content (Morris and Lasek 1982, Perrot et al. 2008). In vitro, NFs are long fibrous structures several hundred nanometers (~50-500 nm) in length and aligned parallel to the length of the axon (Rammensee et al. 2007; Beck et al. 2010). Examination of electron microscope (EM) image of axonal cross-section reveals that, NFs are spaced at" distance (in the range of 30-50 nm) from one another and form an ordered intracellular framework (Hsieh et al. 1994, Kumar et al. 2002 ). NFs are synthesized, assembled in the cell body and trasnported along the axon towards the terminal. In what follows, their structure and assembly characteristics are described.

*2.2.i. Structure and Assembly*

An EM image of the NF purified from spinal cord is shown in the Fig. 2.1a (Janmey et al. 2003). As seen in the figure, NF has a core-shell structure, where the core is formed by the cylindrical backbone. The hairy projections, referred to as the sidearms, radiate from the core of the filament. A schematic representation of the core-shell structure is shown in Fig 2.1b. Though they have a structure similar to other IFs, NFs are unique in terms of their radially extended sidearms.

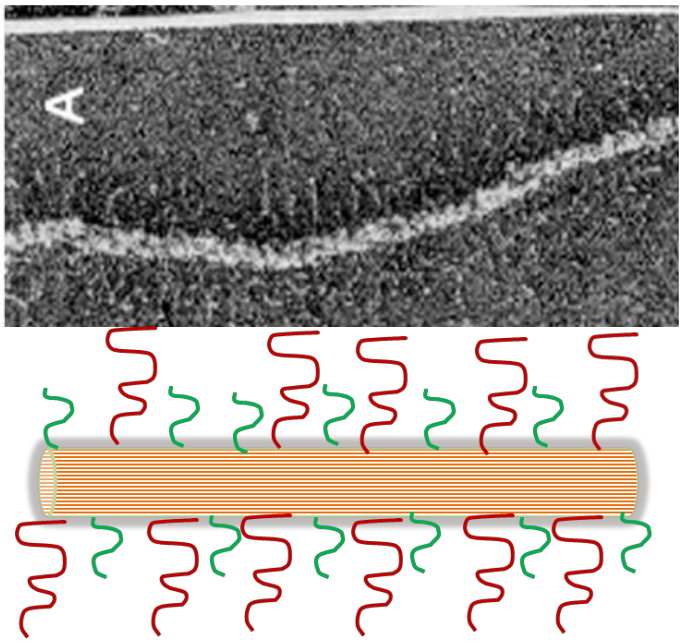


Fig. 2.1 a. Rotary shadow electromicroscope image of single neurofilament. *(adapted from Science 8(1): 40-47 Janmey, P. A., J. F. Leterrier and H. Herrmann (2003). "Assembly and structure of neurofilaments." With permission from Elsiever)* .b. Schematic representation of NF core-shell structure

A fully developed NF is an obligate heteropolymer assembled from three (or four) individual subunits: NF light (NFL; 66 kDa), medium (NFM; 95-100 kDa) and heavy (NFH; 110-115 kDa) (Lee and Cleveland 1996; Perrot et al. 2008), referred as the NF triplets. Additionally, α-internexin and peripherin have been identified as the fourth subunits in the CNS and PNS, respectively (Yuan et al. 2006; Yuan et al. 2012). NF subunits are expressed sequentially at distinct stages of neuronal development. While NFL and NFM are expressed during the initial phases of neuronal differentiation, the expression of NFH is delayed and occurs after the cytoskeleton is stabilized, in concurrence with synaptogenesis. (Carden et al. 1987, Grant and Pant 2000 ). The ratio in which the subunits polymerize to form a single NF is referred as *subunit stoichiometry.* This ratio varies across different species, cell type and developmental stage (Perrot et al. 2008). In a human NF, the stoichiometric ratio of NFL: NFM: NFH is 7:3:2, (Janmey et al. 2003) whereas in mouse it is 6:2:1 (Sanchez et al. 2000). The precise stoichiometric assembly of the subunits is crucial to establish axonal caliber. Accordingly, over or under expression of any of the individual subunits has been linked to inhibition of radial axonal growth (Xu et al. 1996). Altered subunit

ratios have been associated with pathological conditions related to neurodegeneration (Xu et al. 1996, Kim et al. 2011).

The NF subunits share a common tripartite structure consisting of a central α-helical rod domain (~46 nm long) of ~310 amino acids, flanked by N-terminal head and COOH terminal tail domains of varying sizes and sequences. Schematic representation of the structure of NF triplets is depicted in the Figure 2.2. The C-terminal tails of NFM and NFH (~ 514 and 613 residues, respectively, in human NFs) constitute the long flexible polypeptide chains called sidearms that project from the backbone. A relatively short tail (~ 142 residues) is found in the C-termini of NFL proteins. Each domain of these subunits has a specific role in determining the NF physiology. While the post-translational modification of N-terminal domains of NFL and NFM facilitate the assembly, (Heins et al. 1993), the rod domain forms the cylindrical core by polymerizing with rod domains of other subunits. On the other hand, C-terminals are implicated in axonal growth and stability. (Yuan et al. 2012).

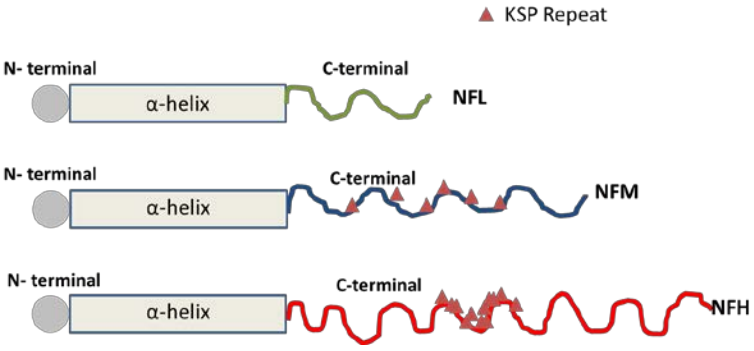


Fig. 2.2. Schematic representation of NF sidearms NFL, NFM and NFH. Each subunit is characterized by Amino terminal (N-terminal) head, central α-helical rod and C-terminal domains as shown in the figures. KSP repeats on C-terminals of NFM and NFH are represented by red triangles)

The NF triplets assemble in a multi-step, sequential assembly process to form a mature NF (Janmey et al. 2003). Briefly, the process involves step by step growth of the polymer, starting with the formation of dimers followed by oligomeric complexes and finally leading to the growth of mature

filamentous polymer. A schematic representation of step by step NF assembly process is shown in Fig. 2.3. In the first step, the central rod domains of NFL assemble with itself or the other two subunits (NFM and NFH) to form a coiled-coil dimer. In this regard, the common α-helical domains consist of highly conserved motifs, where every seventh residue is hydrophobic, that provides a hydrophobic seal on its surface (Fliegner and Liem 1991).

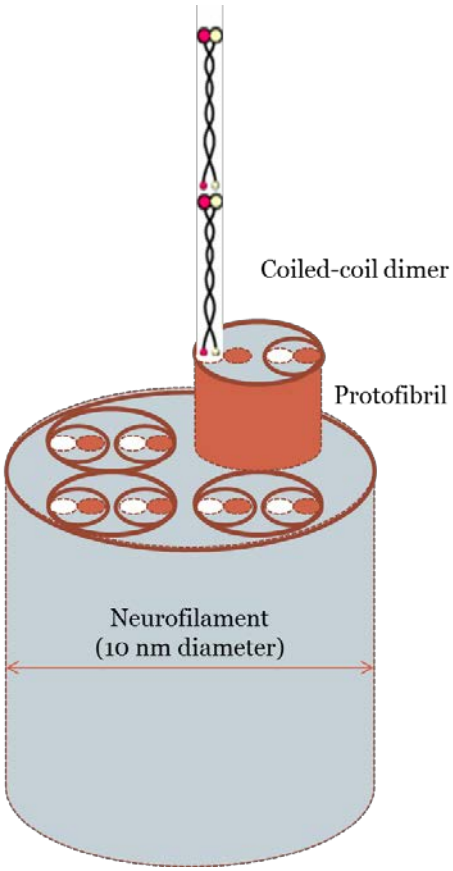


Fig. 2.3. Schematic representation of the multi-step assembly of individual subunits into mature NF. In the first step rod domains assemble to form coiled-coil dimers. Dimers assemble in an antiparallel fashion to form tetramers. The tetramers join in a staggered overlap to form protofibrils which assemble into mature filament.

The interactions between such helical chains aligned in an anti-parallel fashion leads to the formation of a stable coiled-coil structure (Fliegner and Liem 1991). NFL is the only subunit that can self or co-assemble with other subunits, and therefore forms the essential building block of NF. It is to be noted that the ability of NFL to self-assemble may vary across different species (Carpenter and Ip 1996, Carter et al. 1998, Janmey et al. 2003). While it has been established that human NFL can homopolymerize, the ability of mouse NFL to self-assemble is yet to be ascertained (Carter et al.

1998). The coiled-coil dimers so formed assemble in an anti-symmetric, half-staggered manner to form tetramers. The tetramers in turn interact through head to end association to form protofilaments. Three or four such protofibrils combine to form a single unit length NF of 10 nm diameter (Fuchs and Cleveland 1998, Liu et al. 1999, Janmey et al. 2003).

EM studies show that a unit length neurofilament core is ~55 nm long with 32 polypeptides (or 16 dimers) in its cross-section (Heins et al. 1993). In lieu of the anti-parallel half-staggered (or ¾ staggered) (Janmey et al. 2003; Liu et al. 1999), it is believed that, the C-terminals project from the core of the filament at equally spaced intervals. However, different perspectives exist on the subject of the sidearm distributions along the core of the filament. According to one model, the half or ¾ staggered assembly of 45-50 nm length coiled dimers results in the projection of 15-20 sidearms at an interval of 10-22 nm (Janmey et al. 2003; Beck et al. 2012). On the other hand, other studies view sidearms as being uniformly distributed along the core of the filament radiating every 3-4 nm (Kumar and Hoh 2004; Zhulina and Leermakers 2007). While EM studies provide evidence to both models (Hirokawa 1982; Heins et al. 1993), it remains unclear to what extent the periodicity and distribution of sidearms exerts its influence on the behavior of NF brush.

*2.2.ii. Properties of NF sidearms*

The C-terminals of NFL, NFM and NFH are characterized by distinct length, amino acid sequence and charge characteristics. While NFL forms a protrusion that is particularly rich in glutamic acid residues, NFM and NFH are rich in proline (6.2 % in NFM and 13% in NFH) (Wootton and Federhen 1996). Overall, the aminoacid composition includes polar, apolar, charged and neutral residues. The number of charged amino acid residues as well as the length and stoichiometry of the NF sidearms varies for different species. Table 2.2 summarizes the properties of human and mouse NF sidearms.

Table 2.2. Sidearm properties of the three mouse and human NF proteins
*(Adapted from Stevenson et al. 2011 with permission from Elseiver)*

| Property | Subject | Sidearm type | | |
|---|---|---|---|---|
| | | NFL | NFM | NFH |
| Number of residues in the C-terminal tail | Mouse | 146 | 438 | 679 |
| Stoichiometry | Mouse | 6 | 2 | 1 |
| Number of side arms | Mouse | 21 | 8 | 4 |
| Number of phosphorylation sites | Mouse | 0 | 7 | 51 |
| Charge, dephosphorylated | Mouse | -36 | -64 | -8 |
| Charge, phosphorylated | Mouse | -36 | -78 | -110 |
| Number of residues in the C-terminal tail | Human | 143 | 504 | 607 |
| Stoichiometry | Human | 7 | 3 | 2 |
| Number of side arms | Human | 18 | 8 | 5 |
| Number of phosphorylation sites | Human | 0 | 13 | 40 |
| Charge, dephosphorylated | Human | -35 | -52 | -2 |
| Charge, phosphorylated | Human | -35 | -78 | -82 |

In human NFH, there are 607 amino acids, of which 310 are charged residues, including 156 anionic and 154 cationic residues. On the other hand, out of 504 residues of human NFM, there are 238 charged residues. Among these, 145 are anionic and 93 are cationic residues. Due to the presence of a combination of charged residues the C-terminals behave as polyions, sensitive to changes in ionic concentration, pH, and influx of ions in the intracellular milieu. In case of human, NFH is a neutral polyampholyte (-2e) due to the presence of equally charged (anionic and cationic) residues, while NFL and NFM are non-neutral polyampholytes (-35e and -52e), respectively. Where, e is the elementary charge. In addition to the charged residues, posttranslational modifications, especially phosphorylation of C-terminals further influences the net charge.

NFs are subject to several posttranslational modifications (PTM) that determine their physiology. They are phosphorylation, O-glycolisation, nitration, oxidation and ubiquitination. Among these, phosphorylation is the most important and widely investigated PTM due to high

prevalence of phosphorylation sites on NF and the role of abnormal phosphorylation in neurodegenerative disorders.

*2.2.iii. Phosphorylation*

Being extensively phosphorylated neuro-proteins, every aspect of NF biology, is regulated by phosphorylation (Hisanaga et al. 1990; Nixon et al. 1994; Ackerley et al. 2003). The targets of phosphorylation are located on N-terminal and C-terminal domains of NFL, NFM, and NFH. Each of these domains corresponds to a particular function relating to assembly, transport and axonal elaboration. Within the neuron, the level of phosphorylation is spatially and temporally regulated by the influx of a number of second messenger dependent and independent kinases and phosphatases (Grant and Pant 2000). The activity of phospho-kinases follows a regional gradient that is attributed to the modulation of NF function specific to each cellular region (Grant and Pant 2000, Perrot et al. 2008). Accordingly, while axons are packed with phosphorylated NFs, while the cell body and dendrites have little or none (Nixon and Shea 1992, Nixon et al. 1994) .

In vivo studies on the retinal ganglion cells of the mice reveal that, the head domains of NFL and NFM are phosphorylated by Protein Kinase A, C and N following their synthesis in the cell body (Sihag and Nixon 1989). Phosphorylation of particular sites on head domain was shown to inhibit assembly with other subunits (Hisanaga et al. 1990, Sihag et al. 1999).Therefore, phosphorylation plays an inhibitory role, so as to prevent the premature assembly of NFL thereby facilitating proper integration of other subunits NFM and NFH (Sihag et al. 1999). In agreement with this, it was observed that the transgenic mice with NFL mutated to mimic permanent phosphorylation (by mutating serine to aspartate) exhibit altered NF assembly and decreased axonal transport (Yates et al. 2009). Prior to the entry of NFs into the axon, the phosphates are rapidly overturned (i.e. head domains are dephosphorylated) initiating the process of assembly (Sihag and Nixon 1991).

As the mature NFs are transported along the axon, phosphates are extensively added to the C terminal domains of the NFs of NFM and NFH by the proline directed kinases (Veeranna et al. 2011). The targets of C-terminal phosphorylation are the highly conserved Lysine-Serine-Proline (KSP) motifs. NFH of large diameter neurons contains highest number of KSP sites (approx. ~8-58 motifs depending on the species) (Shetty et al. 1993). The addition of phosphates to the KSP motifs converts the charge of serine from +1e to -1e. In human NFM and NFH sidearms that consist of 13 and 40 KSP sites, respectively, the net charge increases from -2e to -82e in NFH and from -52e to -78e in the NFM sidearms. The increase in negative charge induces a shift in the charge density distribution. As a result, the sidearms adapt an extended conformation due to local electrostatic repulsions. Evidence to phosphorylation mediated sidearm expansion was provided by rotary shadow microscopy that demonstrated an increase in sidearm expansion by almost 50% (61 to 92 nm) with phosphorylation (Gou et al. 1998). This lateral extension of the sidearms is correlated to increased interfilament spacing in vivo and the expansion of axonal diameter (Carden et al. 1987, Dewaegh et al. 1992, Hsieh et al. 1994, Nixon et al. 1994).

As mentioned earlier, the enzymatic phosphorylation of NFs is regulated by the activity of kinases and phosphatases. The signaling pathways that activate these kinases are concurrent with myelination and synaptogenesis. Multiple studies have established the correlation between myelination and phosphorylation. When compared to unmyelinated regions such as nodes of Ranvier, myelinated neurons have highly phosphorylated NFs and relatively large axonal caliber (Reles and Friede 1991, Mata et al. 1992). Trembler mutant mice marked by the presence of demyelinated neurons showed decreased phosphorylation levels when compared to their controls (de Waegh et al. 1992). Similarly, mice deficient in myelin associated glycoprotein (MAG) were reported to have decreased levels of phosphorylation and axonal caliber (Dashiell et al. 2002). From these and later studies, it is expected that local interactions between myelinating glia and axons activate the enzymes responsible for the phosphorylation of NFs (Yin et al 1998).

Several studies implicated phosphorylation of N and C-terminal of having a key role in assembly, transport and radial growth. In addition, phosphorylation confers exceptional proteolytic resistance to NFs (Pant 1988). Abnormal accumulation of hyperphosphorylated neurofilaments has been associated with pathogenesis of several motor neuron diseases (Perrot and Eyer 2009). On the other hand, hypophosphorylation has been observed in demylenated axons in multiple sclerosis (Petzold et al. 2008) . Although it is known that the topographical phospho-regulation of NFs has a specific role, there are several open questions pertaining to its activity. Especially, C-terminal phosphorylation of NFM and NFH is being extensively investigated in relation to axonal growth and NF transport through the axons. An understanding of the molecular mechanisms underlying the modulation of NF properties C-terminal phosphorylation is expected to provide insights into the radial growth and maintenance of axonal caliber by NFs.

*2.2.iv. NF Transport*

After their synthesis in the cell body, neuronal proteins are transported to the axon terminal and dendrites through the axon. Radio isotopic labelling studies in mice sciatic nerve reveal that membranous organelles such as mitochondria, ribosomes and neurotransmitters undergo fast transport (~250-300mm/day) by associating with molecular motors belonging to family of kinesin and dynein. On the other hand NFs, MT and other cytosolic proteins move at a slow rate (~0.1 to 2mm/day) (Lasek et al. 1992, Nixon 1998). The slow transport of NFs is accompanied by the phosphorylation of the C-terminal domains and their integration into a stationary network. Investigation of NF motility in cultured nerve cells using green fluorescent protein (GFP) labeling studies revealed that the slow transport of NFs is a consequence of intermittent fast bidirectional movement followed by intermittent long pause (Wang et al. 2000) resembling a “stop and go” model (Brown 2000). It is inferred that at any given time, a small pool/bundle of NF move across

the axon at a slow rate of transport through an existing stationary network of cytoskeletal filaments. (Yuan et al. 2009, Yuan et al. 2012).

An important concern with regards to the slow NF transport is what determines the rate at which they move? Given that the slowing of the transport is accompanied by C-terminal phosphorylation it was speculated that the rate of transport of NFs is somehow regulated by phosphorylation. (Hoffman et al. 1983). Central to this hypothesis is the finding of relatively fast movement of hypophosphorylated NFH in mouse optic axons when compared to hyperphosphorylated NFH (Lewis and Nixon 1988, Jung et al. 2000) . In a different study by Zhu et al it was observed that disruption of NFH gene accelerates NF transport (Zhu et al. 1998). To further confirm the role of phosphorylation, the rate of transport in axons, where NFH was mutated to emulate permanent phosphorylation was compared to mice with non- phosphorylated NFH (Ackerley et al. 2003). It was observed that the permanently phosphorylated NFs exhibit slower transport rates when compared to phosphorylated mice (Ackerley et al. 2003). Taken together, the studies supported the role of NFH phosphorylation in the rate of NF transport (Marszalek et al. 1996, Zhu et al. 1998, Ackerley et al. 2003). On the contrary, different results emerged from studies by Rao and colleagues that specifically examined the role of phosphorylation in axonal growth and NF transport in transgenic mice by deleting the NFM and NFH sidearms. The studies revealed that the deletion of NFM or NFH tails (Yuan et al. 2006) did not influence the rate of transport (Rao et al. 2002, Rao et al. 2003). These unprecedented results called for further exploration into the exact role of the NF sidearms and their subunits in regulating NF transport.

The other important question is what are the molecular motors that drive the NF? It is known that fast axonal transport of other neuronal proteins is mediated by their association with motors belonging to Kinesin and Dynein family (Shah and Cleveland 2002). However, in case of NFs, the molecular motors that modulate the rate of transport are yet to be identified. Originally, it was

believed that MT associate with the fast molecular motors (kinesin and Dynein) and NFs tag along with MT as they move (Craciun et al. 2005). Though it has been identified that NFM and NFH associate with the same motors (kinesin and dynein), their "alternating bursts" of movement followed by pause was different when compared to continuous movement of other proteins which associate with these motors. In this regard, the studies by Yabe et al suggested that NF phosphorylation may have a control over the association and dissociation of the molecular motors. (Yabe et al. 2000). It was inferred that the bidirectional movement (anterograde and retrograde) of NFs is made possible by the phosphorylation mediated association with the motors. The gap between the association and dissociation of these motors may have resulted in the long intervals of rest observed (Roy et al. 2000, Wang and Brown 2001, Barry et al. 2007).

There has been extensive investigation into the form in which NFs move along the axon. Two models have been proposed to describe NF transport based on the experimental evidence. In one model the NF subunits are assembled in the perikaryon and move along the axon in a polymeric form (Roy et al. 2000, Wang et al. 2000), whereas the other model proposes that NFs move in the form of free individual subunits and may not be necessarily in an assembled state (Terada et al. 1996). As a direct evidence to the polymeric model, Yan and Brown et al were able to visualize the movement of polymeric forms of NF in the axon of cultured rat sympathetic neurons (Yan and Brown 2005). Some earlier studies reported the transport of isolated NFM subunit at a slow rate supporting the subunit transport model (Terada et al. 1996). This was further confirmed by gene knockout studies by Yuan and colleagues, which demonstrated the slow movement of NFM subunits in mice lacking one or both of NFL and NFH. (Yuan et al. 2003, Yuan et al. 2006). Thus, NFs can move either in an assembled or as subunit depending on the age and location of the neuron (Yuan et al. 2009).

*NF organization in axon*

In axons, NFs are aligned in a parallel to the length of the axon and appear to form a structural framework along with other cytoskeletal elements of the axon. A quick freeze deep etch microscopy (QFDE) image of rabbit nerve cytoplasm is shown in the Figure 2.4a. As seen in the image the interior of the cell is extensively cross-linked networks of filamentous structures. This network acts as a "scaffold" that confers mechanical stability to the axon (Fuchs and Cleveland 1998). A schematic representation of the same is shown in the Figure 2.4b. The cross-sectional view of an axon reveals an organized distribution of NFs spaced at distance estimated between 40-60 nm. The distribution suggests that the laterally extended sidearms of adjacent NFs interact with another to maintain a minimum obligatory distance between their backbones. These NF-NF interactions are an important part of the structural framework that preserves the axonal architecture. Based on discrete observations from various biological studies, several mechanisms have been proposed to explain the mechanism of sidearm mediated NF interactions. As shown in Figure. 2.4a, the EM depicts NF sidearms as struts emerging from the core of NF to form a cross-bridge between adjacent filaments. Based on this observation, it was postulated that NF interactions are based on ionic cross-links between the laterally extended sidearms aligned in an antiparallel order (Gou et al. 1998, Beck et al. 2012). In contrast, Carden (Carden et al. 1987) argued that adjacent NFs interact with each other by exerting repulsive forces on each other due to their negatively charged nature. Yet another viewpoint proposes entropic repulsive interactions between NFs, where adjacent NF sidearms are viewed as polyelectrolyte brushes that exert entropic repulsion on the neighboring brush. (Brown and Hoh 1997). Despite these, the precise nature of interactions remains elusive and is a subject of extensive investigation.

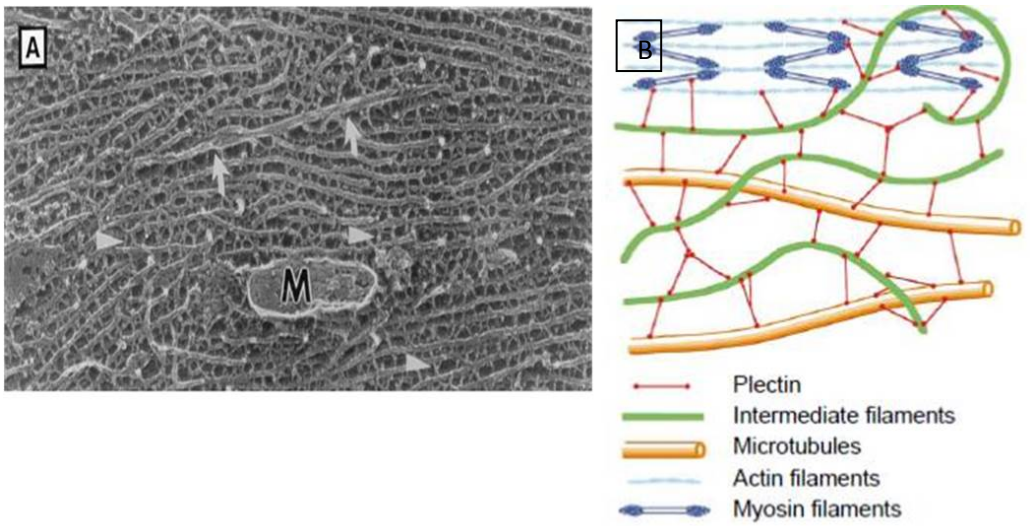


Fig.2.4. a. Quick-freeze deep-etch view of the cytoplasm of a myelinated axon from a rabbit sciatic nerve Adapted from (Fuchs and Cleveland 1998). Microtubules are denoted by curved arrows. Remaining structures are neurofilaments, which are extensively cross-bridged to each other (arrowheads) and to microtubules. b. Schematic representation of the cytoskeletal " structural scaffold". *Figures(a&b) adapted from Fuchs, E. and D. W. Cleveland (1998). "A structural scaffolding of intermediate filaments in health and disease." Science* ***279****(5350): 514-519 with permission from AAAS.*

NFs also interact with MTs that are one of the major participants of the intra-axonal network (Perrot et al. 2008). These interactions are mediated by linker proteins known as microtubule associated proteins (MAPs). The MAPs act by attaching to the several binding sites present on the C-terminal domains. (Hirokawa et al. 1988). Presence of cross bridges between NF and MTs was visualized in vitro by both binding and viscosity studies (Leterrier et al. 1982, Aamodt and Williams 1984). Further, it was observed that dephosphorylation of NF promotes interactions between NFH and MT. Other than MT, NFs also interact with the with several other cytoskeletal filaments including F-actin, myosin, mitochondria and other proteins (Perrot et al. 2008).

### *2.2.v Function of neurofilaments*

NFs have a central role in specifying axonal conduction properties. Their main function corresponds to the growth and maintenance of axonal caliber which in turn determines the conduction velocity. Further, they are the key participants of the intracellular network that imparts mechanical stability to the axon. (Fuchs and Cleveland 1998; Julien 1999; Perrot et al. 2008). NFs

have also been implicated in neuronal development and regeneration (Wang et al. 2012). Post transcriptional regulation of NF gene expression has been closely correlated with axonal growth and repair (Lin and Holt 2008).

*Axonal Diameter*

NFs play a key role in specifying the axonal diameter of large myelinated motor and sensory neurons. The axonal development begins in a post natal stage parallel with myelination and continues through adulthood. During this development, the axons increase in diameter from ~1-2 μm in the early stages to ~14 μm with a corresponding increase in the volume (> 100 fold) (Rao et al. 1998). The expansion of axonal size by up to fivefold is initiated by localized accumulation of NFs, specifically in the myelinated regions of the axon (Jafari et al, 1997). As direct evidence to this, the radial growth of the axons is correlated to marked up-regulation of the NF mRNA and local accumulation of NFs in axons (Muma et al. 1991, Nixon et al. 1994). Further, it was also postulated that myelination promotes the radial expansion by activating kinases that phosphorylate NF sidearms in axons (de Waegh et al. 1992). The "unequivocal" evidence to the correlation between radial outgrowth and NF was provided by study of mutant Japanese quail lacking NFs (Ohara et al. 1993). The quails manifested suppressed radial growth and consequent loss of conduction velocity.

Although it is known that the NFs have a major role in axonal growth, the precise mechanism underlying sidearm mediated expansion remains to be fully understood. In view of the results observed by Ohara et al and their own studies, Friede and Samorajski proposed a linear relationship between NF density and axonal size (Friede and Samorajski 1970). However, it was observed that overexpression of any single subunit suppressed the radial growth disproving the linear relation (Monteiro et al. 1990). Transgenic mice expressing elevated NFL reported little difference in their axon radius, despite of 2-3 fold increase in NF density (Xu et al. 1996). On the other hand, gene deletion studies have demonstrated the absence of NFL leads to a marked

reduction in the levels of NFM and NFH, and diminished radial axonal growth (Ohara et al., 1993; Zhu et al., 1997). Notably, simultaneous overexpression of the three subunits resulted in an increase in the axonal diameter. Collectively, these studies established that NF subunit stoichiometry is critical in specifying the axonal caliber (Xu et al. 1996).

Several lines of evidence have suggested definitive role of C-terminal phosphorylation of NFM and NFH in establishing axonal caliber (Marszalek et al. 1996). Phosphorylation induces structural transitions which rigidify and extend the sidearms (Glicksman et al. 1987). The projected sidearms establish an interaction with their nearest neighbor while maintaining an obligatory distance of 30-60 nm between their backbones (core) (Nixon et al. 1994, de Waegh et al. 1992). The expansion of the axonal volume is correlated to the nearest neighbor distance, established by the C-terminal domains of phospho-regulated network between NFs. A series of investigations were carried out to delineate the mechanism underlying NF mediated radial growth, especially the role of subunits NFM and NFH and the phosphorylation of their C-terminal domains. Elder et al examined the changes in the axonal caliber by generating NFM and H deleted mice (Elder et al. 1998). While lack of NFH did not affect the radial growth, deletion of NFM resulted in diminished axonal calibers (Elder et al. 1998). These observations were supported by similar studies by Rao et al on NFH null mice, which showed that the absence of NFH had minimal effect on the nearest neighbor spacing and the axonal growth (Rao et al. 1998). Further, to investigate the role of C-terminal domains in this regard, Rao et al examined mutant mice by deleting NFH and NFM sidearms (Rao et al. 2002, Rao et al. 2003). The studies revealed that axonal caliber and interfilament spacing remain unaffected by the loss of NFH C-terminal domain (Rao et al. 2002). Taken together, the studies concluded that neither NFH subunit nor its phosphorylation had any influence on axonal growth (Rao et al. 1998). On the other hand, mutant mice lacking in C-terminal of NFM exhibit diminished radial growth (~50%) accompanied by reduction in the nearest neighbor distance (Rao et al. 2003). Therefore, it was implied that the phosphorylation of NFM KSP

repeats is involved in the axonal growth by NFs. Interestingly, when the KSP repeats of NFM were mutated (Serine of KSP motif to Alanine) , the mice did not exhibit any difference in terms of their axonal size or nearest neighbor distance, when compared to the wild type mice thus questioning the validity of the existing hypothesis (Garcia et al. 2009). Moreover, lengthening of NFM C-terminal by addition of amino acids including KSP repeats have resulted in large diameter axons suggesting the expansion of NFM C-terminal as a more likely mechanism (Barry et al. 2012). That said, the exact process underlying the radial expansion by NFM sidearms is yet to be comprehended. Further, the functional significance of intra axonal spacing and the NF mediated sidearm interactions in relation to axonal calibers also remain unsettled.

*Conduction Velocity*

Being the key determinants of axonal diameter, NFs also influence the nerve conduction properties. Conduction velocity is the rate at which action potential is propagated through nerves. It is influenced by three main factors, 1) axonal diameter 2) myelination and 3) internodal length. The conduction velocity varies directly with respect to axonal diameter. Therefore, larger the diameter, the faster the nerve conduction velocity (Hodes 1953). Several studies show that discrepancies in axonal growth due to aberrant NF behavior lead to abnormal conduction velocities. In the study by Ohara et al, the Japanese Quiver quail with mutated NFL expression, exhibit reduced conduction velocity in proportion to axonal caliber. (Ohara et al. 1993, Sakaguchi et al. 1993). This was paralleled by report of conduction loss observed in mutated mice lacking in NFL and NFM C-terminal domains by almost 70% and 30% respectively. (Zhu et al. 1997, Kriz et al. 2000, Garcia et al. 2003). In addition to conduction velocity, the electrophysiological properties of nerves, such as auditory evoked potentials, prolongation of the refractory period, decreased resting membrane potential were also influenced by aberrant NF expression (Perrot et al. 2007). In addition to axonal diameter, myelination exerts significant influence on the conduction velocities. Myelination acts to prevent charge loss and activate biochemical changes that are responsible for the growth of axonal

diameter that exerts influence on the rate of conduction. Therefore defects in myelin formation could influence axonal growth as well as nerve conduction properties (Dewaegh et al. 1992, Ohara et al. 1993, Zhu et al. 1997, Yin et al 1998 ).

*Mechanical Stability*

The interior of an axon is a structural lattice with extensively interconnected structures that confer mechanical stability to the axons and protects them against external compression. NFs and MTs are the major participants of this cytoskeletal framework. The evidence to the resilient nature of NFs is provided by different structural and mechanical studies on isolated axons (McHale et al. 1995, Povlishock and Christman 1995). Rheological studies show that, the NFs form visco-elastic gels that exhibit high elastic modulus (>100 Pa) and the properties of these gels were found to be sensitive to phosphorylation (Leterrier et al. 1996). This observation was also supported by atomic force microscopy (AFM) by demonstrating that the NFs can be stretched up to 3 times their length with an average extension of 2.6 fold upon applying force (Kreplak et al. 2005). In a different study, the NF networks demonstrated an exceptional ability to quickly recover from mechanical disruptions when compared to networks of F-actin (Wagner et al. 2007).

*NF pathologies*

Appropriate expression, assembly, transport and formation of network by NFs are essential for proper neuronal growth. Disruptions in any of these aspects could lead to the abnormal accumulation of NF in neuronal cell. Such accumulated NF networks are the hallmark of various neurodegenerative disorders. Whether they are the pathological reflection of the underlying disease or the causative factor is not completely understood. Several factors can induce abnormal NF accumulations. Among these, NF gene mutation, abnormal post translational modifications, defective NF transport are considered the main factors (Perrot and Eyer 2009).

*NF Pathologies in various neurodegenerative disorders:* Amyotrophic lateral sclerosis (ALS) is a motor neuron disease that leads to progressive loss of muscular movements and neuronal loss. One of the main pathological features of ALS is the presence of perikaryal aggregates of hyperphosphorylated NFs (Manetto et al. 1988). Abnormal NF transport (Lee et al. 1994), altered stoichiometry and irregular activity of kinases that regulate phosphorylation have been correlated to the pathogenesis of ALS . Alzheimer's (AD), one of the most common dementias, is characterized by the presence of neurofibrillary tangles (NFT). The NFs present in these tangles are extensively phosphorylated and are suspected to be caused by down-regulation of phosphatase 2A (Gong et al. 1995, Gong et al. 1993). Lewy body inclusions manifested in Parkinson's Disease also contain NF in addition to ubiquitin, proteasome subunits, and α-synuclein (Forno et al. 1986, Pappolla 1986). Abnormal NF gene mutations have been linked to the onset of Charcoat-Marie-Tooth 2 (CMT2) disease. CMT2 is an inherited neuropathy affecting mainly sensory and motor neurons. In this regard, abnormal mutations of NEFL gene have been reported to cause disrupted NF assembly and transport (Vogel et al. 1985).

*NF Compaction in traumatic brain injury (TBI):* Aggregation of NFs in the form of NF compaction is one of the pathological manifestations of TBI (see Review (Smith et al. 2003, Buki and Povlishock 2006)). Axonal injury triggers a cascade of events starting with focal perturbation, impaired axonal transport, axonal swelling followed by progressive neuronal disconnection. This aberrant signal cascade alters the axolemmal permeability and ionic homeostasis triggering massive influx of $Ca^{2+}$. NF compaction is linked to the degradation of NF network by $Ca^{2+}$ activated proteases. Okonkwo et al examined the morphological characteristics of NF cytoskeleton by subjecting adult cats to TAI (by injecting horseradish peroxidase). It was observed that NF sidearms in injured axons are retracted (shrink) in length (by ~ 50%) when compared to their controls (Okonkwo et al. 1998). Based on these observations, it was inferred that, the presence of excess $Ca^{2+}$ activates kinases responsible for the dephosphorylation of sidearms leading to their collapse. (Okonkwo et al. 1998).

Consequently, the NF interaction is lost followed by the collapse of network that is implicated in interruption of axonal transport. .

In view of the apparent role of NFs in these pathological conditions, it is essential to understand the biochemical mechanisms that trigger their disruptive behavior. Such clear understanding of the mechanisms that effect these changes could help identify potential targets for therapeutic intervention (Smith et al. 2003).

*2.2.vi. Current Research*

In the last decades, experimental and theoretical studies have explored several aspects of NF biology and their implications in neurodegenerative disorders (Perrot et al. 2008 for review). Especially, the transgenic mouse models have advanced our understanding on the role of NF in modulating neuronal function. The transgenic studies involve the application of genetic engineering techniques to modify or delete a particular gene to study the related effects on function of the gene. With regard to NFs, these methods were applied to generate knock out or double knockout mutant mice by modifying gene responsible for the expression of one or two of the subunits of NF (NFL, NFM and NFH) without altering NF stoichiometry. Collectively, the results of these studies have highlighted the distinct roles of each subunit in the NF assembly, transport and radial axonal growth. More importantly, the methods allowed the effect of C-terminal phosphorylation on NF structure and function to be examined. The main results of these studies and their pathological implications are summarized in Table 2.3.

Table 2.3. Summary of transgenic mouse studies.

*(Part of data was adapted from Perrot et al, 2008.)*

| Mice | Axonal Caliber | Axonal Transport | Pathological condition |
|---|---|---|---|
| NFL -/-(Zhu et al. 1997, Yuan et al. 2003) | Decreased by ~ 50% (In L5 ventral root at 2 months old) | Normal Axonal transport of NFM protein | 20% Axonal loss Perikaryal accumulation of NFM and NFH Delayed axonal regeneration |
| NFM -/-(Jacomy et al. 1999) | Decreased by ~ 50% (In L4 ventral root at 3 months old) | Axonal transport of NFL&H increased by two fold in sciatic nerve and five fold in ON | 10% loss of motor axons |
| NFH -/-(Rao et al. 1998, Zhu et al. 1998) | Minor Change | Increased rate of NF transport. | 13% loss of motor axons and 19% loss in sensory axons |
| NFL:NFH -/-(Yuan et al. 2003) | Decreased | NFM transport at normal rate | None |
| NFM:NFH -/-(Elder et al. 1999, Elder et al. 1999) | Decreased by 30-40% (In L4 and L5 ventral root) | Elevated velocity of NFL proteins in sciatic nerve | 24% loss of Motor axons |
| NFM tail deleted (Rao et al. 2003) | Decrease in L5 ventral root at 2 and 6 month old | Normal | None |
| NFH tail deleted (Rao et al. 2002) | Normal in L5 ventral root | Normal | None |

While transgenic models have confirmed the role of NF in axonal expansion, the molecular mechanisms through which NF subunits mediate the growth in vivo are not known. Specifically, an understanding of the relation between the NF morphology and function and how this changes in health and disease is lacking. Our current understanding is based on structural level changes in NF sidearms. In order to correlate these structural transitions to the function, knowledge of subtle biochemical controls which influence their molecular organization is required. Advances in modeling and simulation techniques have enabled us to understand the behavior of such complex systems at different length scale, including atomistic /and molecular level that may not be accessible under conventional experimental methods.

In the recent years, the polyampholytic nature of NFs has inspired the study of NF structure based on the principles of polyelectrolyte brush theory (PEB). In these studies, NFs are treated as polyelectrolyte brush wherein the NF sidearms are the unstructured polyelectrolyte chains that project from the surface of the core. Various models with different levels of complexity have been employed that utilizes 1) Monte-Carlo 2) Self consistent Field theory 3) Molecular Dynamics methods to study the properties of NF brush. The following paragraphs describe these studies concisely.

Monte-Carlo(MC): Polyelectrolyte brush model by Kumar et al employed MC simulations to study the interactions between NFs. (Kumar et al. 2002). MC methods are employed to generate equilibrium structure by sampling the possible configurations based on statistical measures (Smit 2002). In short, the method is implemented in two steps: 1) a random starting configuration is generated and starting energy is calculated. 2) Certain standard moves are implemented (Metropolis MC moves) by applying periodic boundary conditions and the energy ΔE is calculated. The move is accepted or rejected based on probability given by Boltzmann factor $e^{-(\frac{\Delta E}{kT})}$. Thus an equilibrium structure is arrived by sampling a number of such configurations (Smit 2002). In the

model by Kumar et al, NFs were represented as two dimensional disks in canonical ensemble which allows for various representations of the sidearm including telechelic brush, polyelectrolyte brush and neutral polymer brush.

Self-consistent field Method (SCF) : The SCF model incorporated by Zhulina and Leermarkers, is a one dimensional coarse grained model based on mean field approach (Zhulina and Leermakers 2007). According to the mean field theory, a large body of interacting molecules is approximated into a single body by averaging the effect of all the interacting molecules. The model applies mean field theory to smear the sequence based charge distribution of NF sidearms across the backbone. The study shed light onto the organization of NF sidearms under different phosphorylation states at varying pH and ionic conditions.

Molecular Dynamics (MD): Stevens et al investigated the conformational dynamics of NF sidearms and the behavior of interacting NF brushes that are grafted to a planar surface, by performing MD simulations (Stevens and Hoh 2010, Stevens and Hoh 2011). MD simulations reveal the dynamic behavior of a system as a function of time where, the trajectory of the moving particles is calculated is by integrating Newton's equations of motion. The NF brush in their study was modeled based on a coarse grained approach, wherein the sidearms are treated by bead-spring representation. The residues of the NF sequence are represented by beads assigned with one of the four types i.e. positive, negative, hydrophobic and hydrophilic. The study provided insights into the dynamics of interacting NF brushes.

In addition to these, mathematical models were also developed to explain transport of neurofilaments in axons (Yan and Brown 2005). This model is based on mass conservation of concentrations of NFs as they move along the axon. The kinetic parameters were obtained from experimental measured by Wang and Brown et al (Wang and Brown 2001).

*2.2.vii Summary and Research objective*

To summarize, studies in animal models and theoretical studies have shed light onto certain key aspects of NF biology and their relation to neuronal function. The main results of these studies are as follows: Gene knockout studies have shown that over or under-expression of any of the subunits can severely impede the assembly and physiological properties of NFs. While NFL is critical for assembly (Gill et al. 1990), NFM and NFH have a regulatory role in the NF transport and in specifying the axonal diameter (Garcia et al. 2003, Rao et al. 2003, Garcia et al. 2009). Especially, NFM has been identified as the key player in mediating interactions with adjacent filaments and consequently the radial growth of axons (Rao et al. 2003), while NFH has more of a modulatory role. Further, It has emerged that phosphorylation of NFM C-terminal domain may not be essential for axonal growth (Garcia et al. 2009). While the ongoing studies have shed light into several aspects of NF physiology, they have also raised some new questions. For example: what is the precise nature of NF-NF interactions which govern the axonal network and what are the parameters which modulate the strength of these interactions? Though the experimental studies suggest a dominant role of NFM in modulating the axonal diameter, the precise mechanism by which these sidearms mediate the axonal growth is yet to be understood. Another important question is the role of localized enzymatic phosphorylation in the sidearm mediated NF expansion. Originally it was anticipated that phosphorylation has a predominant role in axonal growth. However, recent studies have indicated otherwise. In view of this, a deeper understanding of the role of phosphorylation is essential. In this work we investigate some of these questions.

The overall goal of our research is to understand the structural and biophysical basis of NF organization. Multi-scale computational models that incorporate electro-physiological characteristics of NFs have been instrumental in revealing some of these aspects. By utilizing a combination of 3D coarse grained model of NF and an atomistic model of the NFM polypeptide

which incorporate the molecular level organization of the sidearm, a theoretical perspective of molecular mechanisms underlying their behavior could be obtained. NF-NF interactions are implicated in regulating axonal biomechanics, radial growth and transport. The "physical basis" of these interactions has been the subject of several of experimental and theoretical studies. However, a clear consensus on the exact nature of interactions is lacking. Under ***specific aim 1***, we attempt to gain insight into the nature of sidearm-mediated neurofilament interaction. The conformational features of a NF are sensitive to changes in the cellular environment such as influx of ions or change in pH due to the polyampholytic nature of their C-terminal domains. Under ***specific aim 2***, with the aim of understanding the conformational dynamics of sidearms in response to different physiological conditions, we investigated the effect of $Ca^{2+}$ ions on the structure of the human NF under the influence of varying ionic strengths. Further, the sidearms consist of a number of hydrophobic moieties, whose influence on the NF structure is not clear. Therefore, as part of this study, we also investigated the effect of hydrophobic interactions on the conformational properties of human NF. ***Specific Aim 3*** is aimed at gaining molecular level understanding on the role of KSP repeat phosphorylation on the conformation of NFM C-terminal polypeptide. To accomplish this, all-atom Molecular Dynamics simulations of mouse and mutated mouse NFM sidearms were performed at different phosphorylation conditions at physiological ionic and temperature conditions.

# Chapter III

## Conformational properties of interacting neurofilaments: Monte Carlo simulations of cylindrically grafted apposing neurofilament brushes

*This work was published in (Jayanthi et al. 2013)*

### *3.1 Introduction*

Side-arm mediated NF-NF interactions are implicated in the expansion of the axonal diameter and structuring of the axoplasm. The mechanical nature of interactions between NFs and the physiochemical controls which modulate their strength or trigger their collapse are not very well understood. Several theoretical and experimental studies have been carried out to investigate NF organization by examining NF network properties. Taken together, three models have been put forth to explain the interaction mechanism.

The first model describes NF-NF interaction in terms of cross-bridge formation between adjacent filaments (Hirokawa 1982, Hirokawa et al. 1984, Leterrier et al. 1996, Gou et al. 1998). In this model, the non-covalent binding of NF sidearms, either by themselves or mediated by other accessory agents, is considered to be responsible for NF interactions. This hypothesis was originally based on EM studies of the frog axon where sidearms were found to form a dense network of cross-bridges that were 4-6 nm in diameter and 20-50nm in length (Hirokawa 1982; Leterrier et al. 1996). In a recent study, Beck et al. proposed that the sidearms are locked in a hand-shake type of interaction mediated by ionic cross-linking between the charged residues of the sidearms, supporting the cross-bridge model (Beck et al. 2012)

In the second model, the sidearm-mediated interfilament interaction is described in terms of repulsive electrostatic interaction (Carden et al., 1987). This hypothesis was based on the observation that NF sidearms are abundant with ionizable amino acid residues. In particular, the net negative charge attained from serine phosphorylation of the KSP repeat motifs was considered

to be responsible for sidearm-mediated NF interaction, suggesting that the interfilament spacing between NFs is regulated by electrostatic repulsion (Carden et al., 1987; Dewaegh et al., 1992).

A third model sees the interfilament interaction as akin to the entropic repulsion in a polymer brush (Brown and Hoh, 1997; Kumar et al., 2002), with the NF sidearms acting as unstructured polyelectrolytes that experience mutual steric exclusion through short-range repulsions. The hypothesis for this model was based on the atomic force microscopy measurement that revealed the exclusion of co-assembled material from the proximity of the NF core and the presence of weak repulsive forces that extend for more than 50 nm from the filament core (Brown and Hoh, 1997).

NF sidearms have an abundance of positive and negatively charged residues, which is attributed to their polyampholytic nature. In the past, different studies have employed conformational analysis to shed light into the nature of interacting polyelectrolyte brushes (Korobko et al. 2004). For example, Cao et al. employed coarse-grained bead spring polymer brush model to computationally study the conformational characteristics of polyelectrolyte brushes that are end-grafted to two apposing planar surfaces (Qianqian cao 2009). A similar study investigated a pair of spherical polyelectrolyte brushes (SPEs) to assess the behavior of chain conformations when subjected to compression under low and high ionic concentration solutions (Korobko et al. 2004). Both studies revealed coiled conformations under high ionic concentrations, giving insight into the dynamic properties of polyelectrolyte brushes under ionic conditions.

Compared to pure polyelectrolyte brushes, the nature and charge distribution of NF sidearms provide rich conformational behavior that may play an important role in controlling the interactions between neighboring filaments. Such behavior was addressed by the recent work of Stevens et al. who examined the interactions between apposing NF sidearms that are grafted to planar surfaces (Stevens and Hoh 2010, Stevens and Hoh 2011). The study revealed that the sidearms adopt a condensed conformation and exhibit significant interdigitation upon compression

of the walls. In our study, a model of cylindrically grafted apposing NF sidearms was treated to reveal the conformational properties of interacting NFs. The model comprises a cylindrically grafted polypeptide chains representing the 10-nm-diameter NF cores and polyampholyte sidearm chains that are end tethered to the cores according to the stoichiometry of the three NF subunits.

*3.2 Method*

Computational Model

Several computational models have been proposed to study the equilibrium structure and organization of NFs based on PEB brush theory. Usually, the polyelectrolyte or polyampholyte systems are treated either as blocks of uniform charge or homogenous linear distributions. However, the NF sidearms are characterized by inhomogeneous distribution of ionizable charged residues. In addition, phosphorylation acts as a graded switch that provokes a transition in the charge distribution that can influence the lateral sidearm structure. Furthermore, the variations in stoichiometric ratios of the subunits and the distribution of C-terminal domains along the backbone (grafting density) also determine the equilibrium structure of NF through interplay of electrostatic and entropic interactions. All these features add to complexity of modelling NF structure when compared to the simplified representation of other polyelectrolytic systems. In view of this, a computational model which accommodates the NF stoichiometry, grafting density, sequence and charge characteristics that represents the NF in phosphorylated and dephosphorylated states is expected to provide insightful details of their conformational properties under varying environmental conditions.

Taking into consideration all the above features, Chang et al (Chang et al. 2009) developed a 3D coarse-grained model that incorporates the sequence and stoichiometry of human NF. The model is an extension of SCF model developed by Zhulina and Leermakers (Zhulina and Leermakers 2007) and is designed to capture the electrostatic, entropic and hydrophobic interactions between

the residues. To emulate the physical system, the stoichiometry and grafting density were included. A schematic representation of the model is shown in the Figure 3.1.

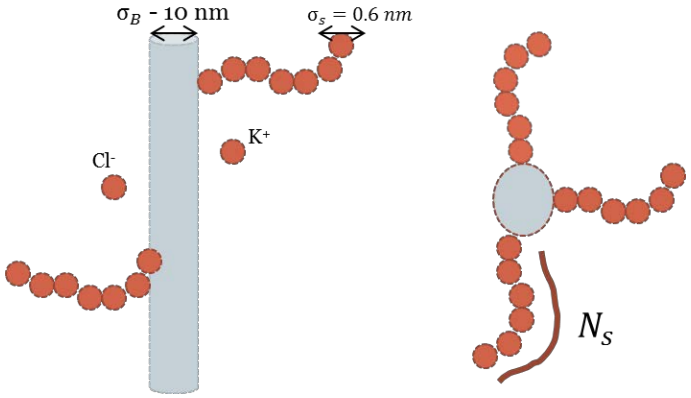


Fig. 3.1 Schematic representation of the model: Ns – amino acids on each chain; $\sigma_B$ – backbone diameter; $\sigma_s$ – amino acid diameter; K+ monovalent counterions for charge neutrality.

In this model, the NF backbone is modelled as a central rod, of diameter $\sigma_B$ = 10 nm and the chains representing sidearms are tethered to the core. The sidearms are modeled as chains consisting of a collection of coarse-grained (CG) sites. Each CG site represents an amino acid residue, according to the number and sequence of the human NF sidearms. The amino acid sequences of human NF and the dimensions (diameter) of the CG sites were adapted from Zhulina et al (Zhulina and Leermakers 2007) with some modifications specific to the sequence. Each CG site was modeled as a hard sphere of diameter $\sigma_s$=0.6 nm, with the corresponding charge valence. The counter-ions K+ were also modeled as hard spheres of diameter as the CG sites. The counterions were added to maintain the charge neutrality of the system under salt-free condition. In the present study, the charge distribution of the CG sites along the sidearm polypeptide is represented based on the side-chain charges (positive, negative, and neutral) of the amino acid residues of the sequence.

For our study, we extended the model developed by Chang et al (Chang et al. 2009) to a pair of cylindrically grafted apposing NFs in order to characterize the conformational changes of NF sidearms in the presence of interacting adjacent filaments. In our model, the NF cores of the two filaments are placed in a box of dimensions 400 nm x 400 nm x 50 nm equidistant from the center of the box, with the filaments axes aligned along the z-axis. A total of 31 sidearms were tethered to each filament core according to the stoichiometric ratio NFL: NFM: NFH of 7:3:2. Therefore, there are 18 NFL, 8 NFM and 5NFH per filament. In each filament, the sidearms were equally spaced along the z-axis of the backbone, but grafted randomly around the core. The interfilament distance between the cores is set by adjusting the distance between the centers of the 10-nm-diameter cylindrical cores. Different interfilament separations ranging from 40 nm to 60 nm were selected, and MC simulations of NF pairs were performed for each interfilament separation. In these simulations, the apposing NFs were first equilibrated at 60 nm separation and then gradually compressed towards 40 nm by reducing the distance between the centers of apposing filaments by 1.25 nm per step. At each stage, the pair was fully equilibrated before further reduction in distance or another production run took place. The equilibrated configuration was then used to generate the next configuration with a smaller separation. This procedure was repeated until the interfilament distance of 40 nm was reached.

The MC simulations were carried out under both phosphorylated and dephosphorylated conditions at salt-free and 150 mM ionic salt concentrations. The salt concentration here represents the effect of salt due to monovalent salt ions such as $K^+$ and $Cl^-$ ions. To simulate the effect of phosphorylation, negative charges of -2*e* were assigned to the serine residues of the KSP repeat motifs in the NFM and NFH sidearms, whereas the serine residues were kept neutral for the dephosphorylated condition. The interaction potential between different objects is treated as the sum of hard sphere (or rod) and electrostatic interactions. The hard sphere (or rod) interaction $U_{hs}\left(r_{ij}\right)$ is given by

$$U_{hs}(r_{ij}) = \begin{cases} \infty & r_{ij} \leq \sigma_{ij} \\ 0 & otherwise \end{cases}, \quad (3.1)$$

Where, $r_{ij}$ is the distance between the centers of two objects *i* and *j*, and $\sigma_{ij} = \frac{\sigma_i + \sigma_j}{2}$.

Under salt-free condition, the electrostatic interaction potential $U_{el}(r_{ij})$ is given by

$$U_{el}(r_{ij}) = \frac{e^2 Z_i Z_j}{4\pi\varepsilon_0 \varepsilon r_{ij}} \quad (3.2)$$

Where, $e$, $\varepsilon_0$, and $\varepsilon$ are the electric charge, vacuum permittivity, and the dielectric constant of a solution, respectively, and $Z_i$ is the charge valence of a coarse-grained site *i*. The electrostatic potential $U_{el}(r_{ij})$ can be expressed in terms of the Bjerrum length $l_B$ as:

$$\frac{U_{el}(r_{ij})}{k_B T} = \frac{l_B Z_i Z_j}{r_{ij}} \quad (3.3)$$

where, $l_B = \frac{e^2}{4\pi\varepsilon_0 \varepsilon k_B T}$ ($k_B$ is the Boltzmann constant and $T$ is the system temperature). The Bjerrum length $l_B$ is the separation at which the electrostatic interaction between two elementary charges is comparable in magnitude to the thermal energy scale $k_B T$ and is around 0.7 nm for water at $T$ = 300K.

In the physiological condition, the ionic concentration is incorporated into the model implicitly by the use of the screened Coulomb (Debye-Hückel) potential given by

$$\frac{U_{el}(r_{ij})}{k_B T} = l_B Z_i Z_j \frac{e^{-\kappa r_{ij}}}{r_{ij}} \quad (3.4)$$

where κ is the inverse Debye screening length (McQuarrie 2000) given by,

$$\kappa^{-1} = \sqrt{\frac{\varepsilon_0 \varepsilon k_B T}{2 N_A e^2 I}} \quad (3.5)$$

Here, $N_A$ is the Avogadro number and $I$ is the ionic strength (M). All other variables are the same as defined above. In terms of the Bjerrum length $l_B$, κ can be written as:

$$\kappa^{-1} = \sqrt{\frac{1}{8\pi l_B N_A I}} \tag{3.6}$$

*Simulation procedure*

The study employs the standard canonical ensemble (NVT i.e., constant number $N$ of particles, volume $V$, and temperature $T$) MC simulations. The initial configurations were generated by randomly inserting monomer beads of sidearms, where the monomer beads are placed randomly starting from the site at which the sidearms are tethered to the filament backbone. The standard MC moves including crankshaft, continuum configuration bias, and random rotation, were then applied for the sidearm chains. The trial moves are implemented in a two stage process. Initially, the move is checked to avoid overlap with other particles. If this condition is satisfied, the change in electrostatic energy, $\Delta U$, associated with the move is calculated by using the Ewald summation method (Smit. 2002). The trial move is accepted or rejected according to the probability of $exp(\frac{-\Delta U}{k_B T})$, where $k_B$ is the Boltzmann constant and $T$ is the absolute temperature (K).

The simulation was performed in a three-step process. In the first step, the neutral system (by setting bjerrum length equal to zero) was equilibrated. Then, the neutral system was charged to represent as either dephosphorylated or phosphorylated systems, which was further equilibrated. In the third step, for sufficient equilibration under each condition (phosphorylation state, proximity, ionic strength), the system was equilibrated for three times the equilibration steps needed for a single filament. In other words, 3 x $10^6$ MC steps were performed under each condition before the last equilibrated simulations of $10^6$ steps were carried out as a production run for sampling the average properties. All average properties were calculated from the equilibrated configurations that were sampled at every 1000 MC steps of the production runs. For sufficient

statistics, the monomer density profile, average interpenetration (I) and average brush height (h) were determined from six independent simulations that were initialized differently. The data presented here represents the average of data collected from six simulations except for the last two distances (i.e. 45 nm and 42.5 nm), where it was averaged over four independent simulations. The use of four independent simulations (instead of six) for averaging at these two distances was due to the challenge in fully equilibrating the NF pairs as the interfilament separation decreases.

*3.3. Results*

In our study, we set out to reveal the conformational behavior of apposing sidearms of interacting adjacent NFs. To this end, we performed off-lattice MC simulations of NF pairs, which comprises apposing sidearms end tethered to cylindrical geometry cores. The study was done at different interfilament separations ranging from 60 to 40 nm. In the first step, a number of independent NF pair simulations were carried out at 60 and 40nm separations. Then the interfilament distance of each independent simulation was reduced in small steps from 60 nm towards 40 nm.

The choice for the range of interfilament distance was partly motivated by the range of reported NF spacing. In the literature, various interfilament separations (40 – 60 nm (Xu et al. 1996), 35 – 40 nm(Kumar and Hoh 2004), and 33 – 48 nm(Hsieh et al. 1994) were reported under normal physiological conditions. Note that, in our model, the interfilament distances are measured from the centers of the 10-nm-diameter backbones. Therefore, the selected range corresponds to 30 – 50 nm from the filament surfaces, which is nearly within the reported physiological ranges.

At the two extreme interfilament separations (60 and 40nm), MC simulations of NF pair were conducted under different conditions, i.e., phosphorylation states and ionic conditions. First, in order to gain insight into the role of electrostatic repulsions on the conformation and

interactions of apposing sidearms, the MC simulations were performed under salt-free condition. The results from these simulations were then compared with similar simulations under physiological ionic condition.

The simulations under physiological ionic condition were continued for interfilament distances from 60 to 40 nm under both phosphorylation states. The conformational changes arising from different factors were then examined using measures such as the average brush height, mutual interpenetration and density profile. Examination of the conformational characteristics of apposing sidearms resulting from these analyses will allow us to gain insight into the nature of sidearm interactions under different conditions.

*Conformations of apposing NF sidearms under salt-free condition*

It is known that the phosphorylation of NF sidearms at their KSP repeat motifs modifies the charge distribution of both NFM and NFH sidearms and increases their lateral extension (Glicksman et al. 1987, Martin et al. 1999). In view of this, it was hypothesized that phosphorylation plays a key role in specifying the interfilament separation (Hsieh et al. 1994, Nixon et al. 1994). Central to this hypothesis is that the interfilament interaction is governed by sidearm-mediated electrostatic repulsion that arises from the net negative charge (Carden et al. 1987). Clearly, such repulsive interaction is expected to manifest itself in the conformational characteristics of apposing sidearms. To observe the conformations arising from sidearm-mediated repulsive interactions, we performed MC simulations of apposing NF brush under salt-free condition, for both phosphorylated and dephosphorylated states. From the resulting conformation, one would be able to gauge the likelihood of repulsive type of interactions between apposing sidearms. Note that the salt-free condition allows us to observe the effect of electrostatic interaction exclusively.

To observe the conformations arising from electrostatic interaction, we first visually inspect the structures of adjacent NFs by extracting representative snapshots of configurations from

equilibrated MC simulations. Figures 3.2a and b depict typical snapshots of the NF brush pair at 60 nm separation. The figures present equilibrated conformations of the dephosphorylated (Fig. 3.2a) and phosphorylated (Fig. 3.2b) NF pairs under salt-free condition. An interesting feature of these figures is that the sidearms from adjacent filaments are found to bend away from each other leaving a depletion region in between, a behavior suggestive of repulsive type of interactions between apposing sidearms.

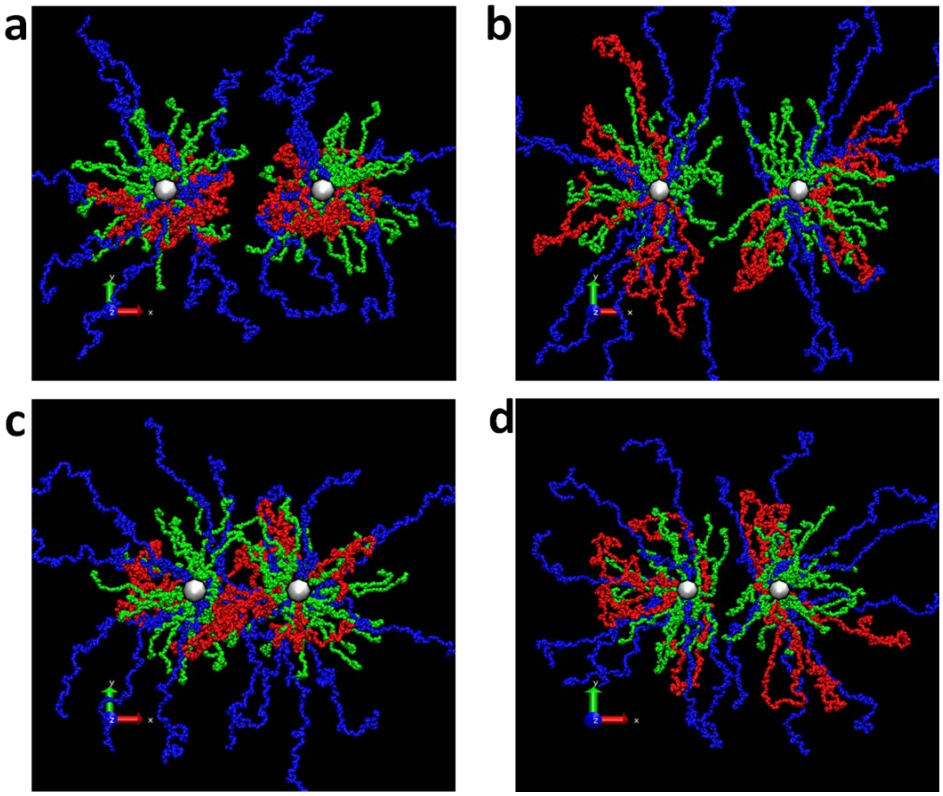


**Fig. 3.2.** Representative snapshots (*top view*) **(a)** of a 60-nm-apart dephosphorylated and **(b)** phosphorylated NF brush pair under salt-free conditions. Snapshots of **(c)** a 40-nm-apart dephosphorylated and **(d)** phosphorylated NF pair under salt-free conditions (color coding: NFL – *green*; NFM – *blue*; NFH – *red*)

The difference between the dephosphorylated (Fig. 3.2a) and phosphorylated (Fig. 3.2b) NF pairs is seen only in the fine tuning present in the individual sidearms. In terms of the individual

sidearms, while NFL and NFM adopt an extended conformation in both phosphorylation states, NFH sidearms exhibit significant changes in their conformation upon change of the phosphorylation condition. Under dephosphorylated condition, NFH sidearms are collapsed around their own filament core, with little to none influence on sidearms from the adjacent filament. In contrast, phosphorylated NFH sidearms adopt an extended conformation with a ring like structure at their free ends and participate in the repulsive interactions.

To observe the effect of proximity on the interacting sidearms, similar MC simulations were performed at 40 nm interfilament separations. Figures 3.2c and d represent the behavior of apposing NFs under salt-free condition when the centers of the filament cores are 40 nm apart. At this separation, one observes a slight difference between the dephosphorylated (Fig. 3.2c) and phosphorylated (Fig. 3.2d) states. In the phosphorylated state, except for the reduction in the depletion region, the apposing sidearms still exhibit a conformation that is indicative of a repulsive type of interaction (cf. Fig. 3.2d). In contrast, dephosphorylated NF pairs exhibit a mixed behavior in which the collapsed NFH sidearms have become mutually interpenetrated, while the other two types of sidearms are expelled out, exhibiting a partially repulsive behavior.

Taken together, under salt-free conditions, NF sidearms from adjacent filaments exhibit conformational characteristics that are reminiscent of repulsive type of interactions as suggested in the literature (Carden et al. 1987, Dewaegh et al. 1992). However, as presented below, this conformational behavior changes significantly when the simulations were performed under ionic solutions, possibly due to a different interaction mechanism.

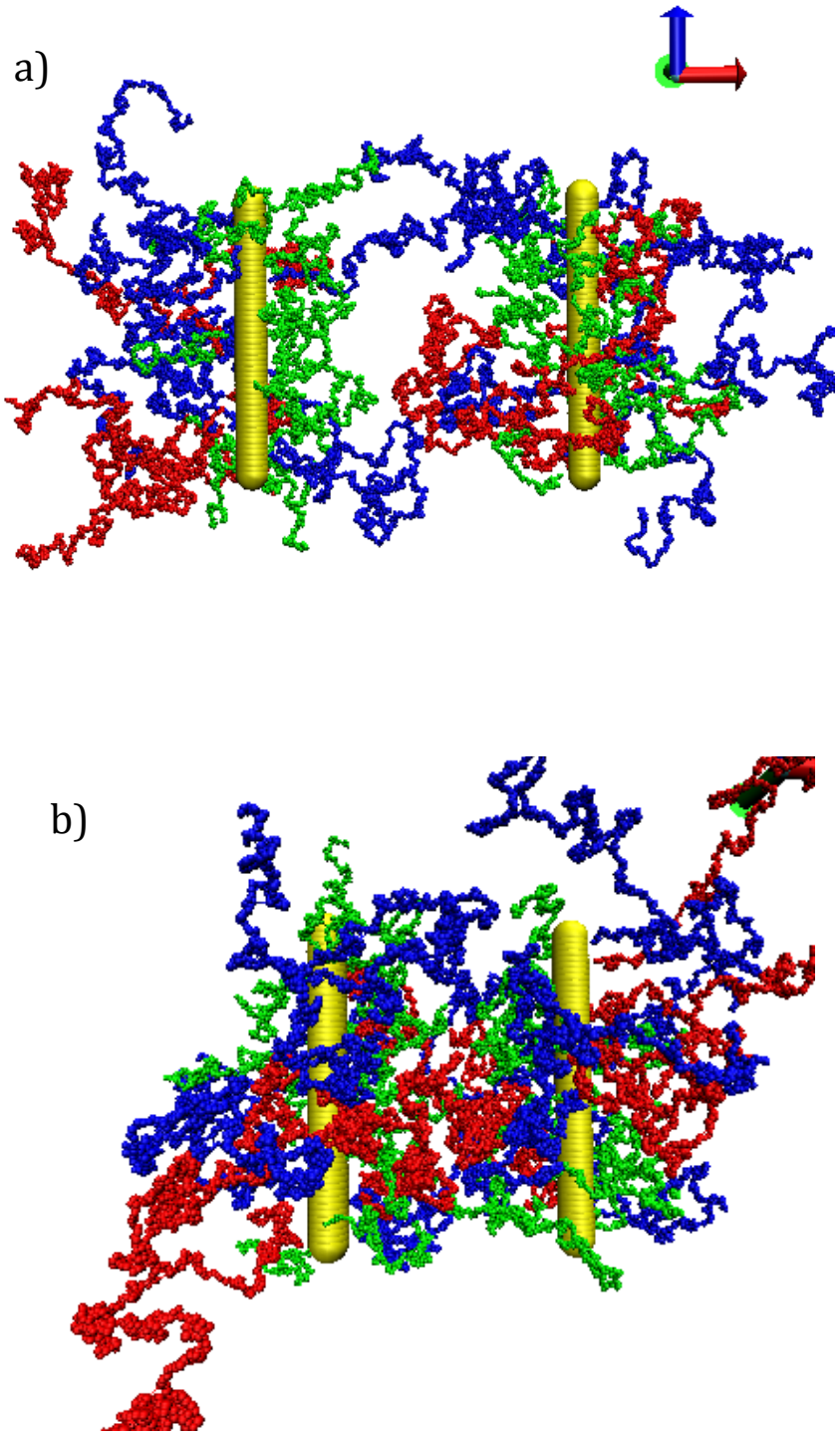


**Fig. 3.3.** Representative snapshots (*side view*) (a) of 60 and (b) 40 nm apart phosphorylated NF brush pair under physiological conditions. (color coding: NFL – *green*; NFM – *blue*; NFH – *red*)

*Conformations of apposing NF sidearms under physiological condition*

The simulations under salt-free condition reveal the conformational behavior of apposing sidearms that can be attributed to repulsive electrostatic type of interactions. They are used as a control to compare the effect of salt concentration. To observe the conformational properties under physiological conditions, we performed MC simulations of adjacent NFs under 150 mM ionic solutions. As commonly practiced in the simulations of polyelectrolyte systems (Panwar and Kumar et al.(Panwar and Kumar 2005) and references therein), the ionic strength is incorporated into the model implicitly through the use of the Debye-Hückel screened Coulomb potential (cf. Methods Section). For comparison with the salt-free condition, the MC simulations were first performed at 60 nm and 40 nm interfilament separations under both phosphorylation conditions

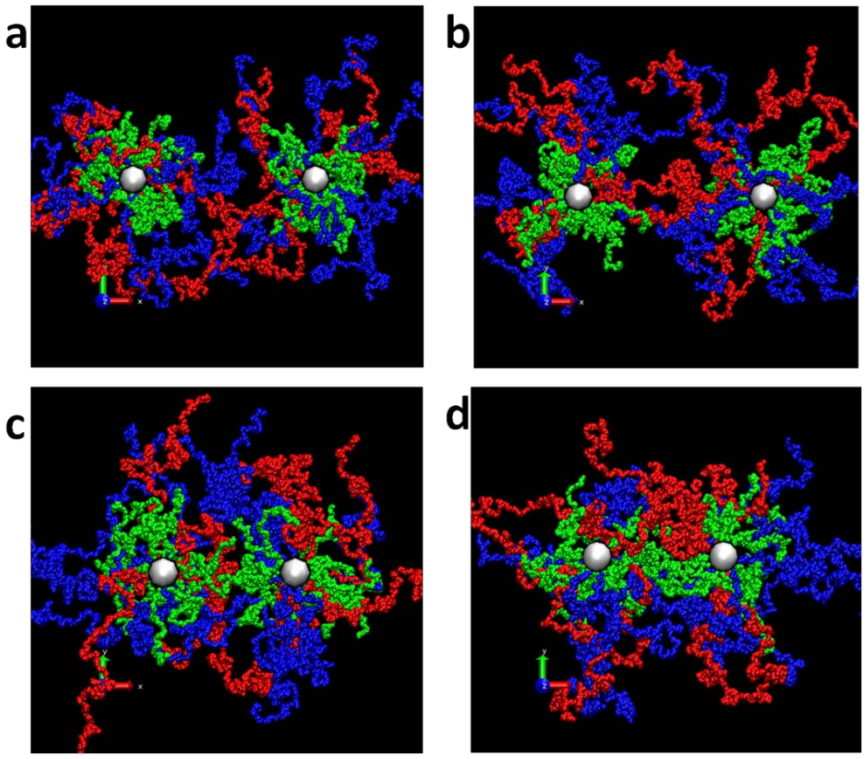


**Fig. 3.4.** Representative snapshots (*top view*) of a 60-nm-apart dephosphorylated (**a**) and phosphorylated (**b**) NF brush pair under physiological condition. Snapshots of a 40-nm-apart dephosphorylated (**c**) and phosphorylated (**d)** NF pair under physiological conditions

Figures 3.3 shows the typical snapshots of the side view of phosphorylated NF pair at 60 nm (a) and 40 nm (b) distance under physiological condition. Figures 3.4a and 3.4b show typical snapshots of the top view of 60 nm apart adjacent NFs under 150 mM ionic conditions. The snapshots depict the equilibrium conformations of dephosphorylated (Fig. 3.4a) and phosphorylated (Fig. 3.3(a) and 3.4b) NF pairs. In sharp contrast to the salt-free condition, the snapshots of the NF pair under physiological condition revealed a coiled conformation for both phosphorylation conditions. Moreover, the difference between the phosphorylated and dephosphorylated NF pairs is not significant at 60 nm separations.

Qualitatively similar behavior was observed for the 40 nm apart neighboring NFs (Fig. 3.3 (b), Fig. 3.4(c, d)). At 150 mM ionic concentration, the apposing sidearms adopt a coiled conformation for both phosphorylation states. However, similar to the salt-free condition, relatively higher mutual interpenetration was observed at 40 nm separations when compared to the 60 nm separations.

The difference in the conformational properties of NF sidearms under 150 mM and salt-free conditions arises from the ionic screening present in the 150 mM ionic solution. In the presence of salt ions, the repulsive interaction observed under salt-free condition will be screened, leading to a type of interaction that is dominated by short-range steric exclusion. When the proximity between the NF cores is reduced from 60 nm to 40 nm, the monomers in each sidearm rearrange themselves so as to relieve the short-range steric repulsions, and eventually adopt a conformation with relatively higher interpenetrations.

*Density profile of apposing neurofilaments*

The above qualitative observations from visual inspection can be quantified through measures that reveal the average properties of sidearm conformation. One such measure is the cross-sectional monomer density profile $\rho(x, y)$ in the apposing sidearms. $\rho(x, y)$represents the

mean distribution of monomers across a planar cross-section normal to the longitudinal axes of the apposing filaments. At any position $\vec{X} \equiv (x, y)$ on the cross-section, $\rho(x, y)$is calculated by counting the number of monomers within the cross-sectional area between $(x, y)$ and $(x + dx, y + dy)$ (for all depth along the longitudinal Z-axis) and then normalizing by the volume, $dxdyL_Z$. Here, $L_z$is the length of the simulation box along the filament longitudinal axis. Mathematically, $\rho(x, y)$can be expressed as

$$\rho(x,y) = \frac{1}{dxdyL_z} \sum_{j}^{N_S} \left\langle \delta\left( \vec{X} - \vec{X}_j \right) \right\rangle \qquad \text{.....} \qquad (3.7)$$

The bracket $\langle \ldots \rangle$ represents the ensemble average, and $\rho(x, y)$is the ensemble average of 1000 configurations sampled from $10^6$ equilibrated MC simulations. The two-dimensional contour plots of the density profile obtained from this calculation, along with the visual data (snapshots), allow us to predict the spatial arrangement of apposing sidearms.

Figures 3.5a and b show the contour plots of $\rho(x, y)$ for the NF pair under salt-free condition. The plot presents the average cross sectional density profiles of 60 nm apart dephosphorylated (Fig. 3.5a) and phosphorylated (Fig. 3.5b) NF pairs. The plots clearly demonstrate that the monomers from one filament are forced to bend away from those of the apposing filament. The monomers in the apposing sidearms are expelled from the central region, forming a depletion region around the center. A similar behavior was observed for the 40-nm-apart NF pairs under salt-free condition. Figs. 3.5c and d represent the average cross sectional density profiles of 40 nm apart dephosphorylated and phosphorylated NF pairs, respectively, under salt-free condition. While the 40-nm-apart dephosphorylated NF pairs show marginal overlapping near the center, the average density profile of the 40-nm-apart phosphorylated apposing sidearms exhibit little mutual interpenetration.

To assess the conformational properties of interacting neurofilaments under physiological conditions and then compare with the salt-free conditions, we calculated the average density profile $\rho(x, y)$ of 40 nm and 60 nm apart NF pairs under 150 mM ionic solutions. Figures 3.6a and 6b depict the contour plots of $\rho(x, y)$ of NF pair at 60 nm and 3.6c and 3.6d of NF pair 40 nm apart in dephosphorylated and phosphorylated conditions, respectively, under physiological conditions. In contrast to the salt-free condition, the plots reveal the coiled conformations of the apposing sidearms. Additionally, noticeable conformational difference was observed between the 40-nm and 60-nm-apart NF pairs.

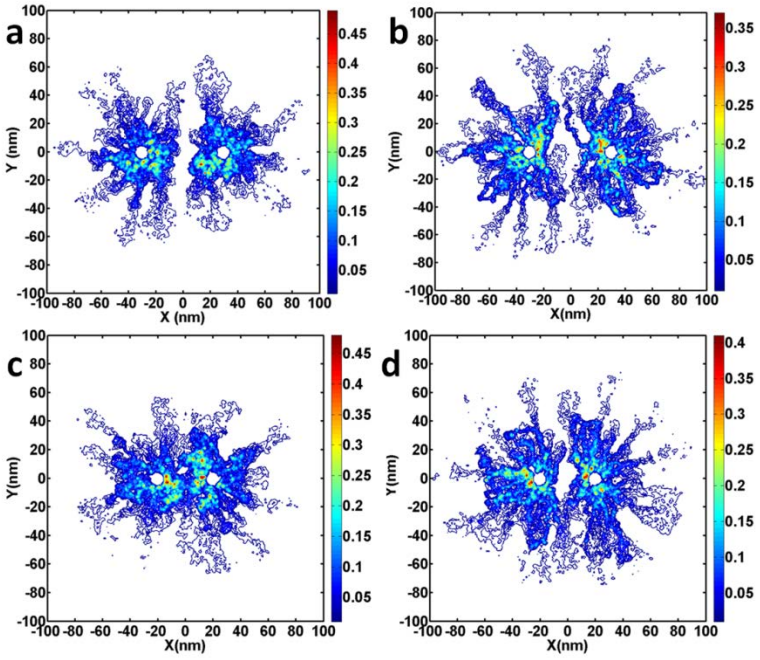


**Fig. 3.5** Two-dimensional contour plots of the average cross-sectional density profile $\rho(x, y)$ of the 60-nm apart dephosphorylated (**a**) and phosphorylated (**b**) NF pair under salt-free conditions. Similar contour plots of $\rho(x, y)$ for the 40-nm-apart dephosphorylated (**c**) and phosphorylated (**d**) NF pair under salt-free conditions

At the 60 nm separations, the density profile reveals that the apposing sidearms aggregated around their own filament core, with marginal overlapping at the center. On the other hand, relatively higher overlapping or interpenetration is observed in the density profile of 40-nm-apart NF pairs

With regard to the phosphorylation state, no significant difference was observed in the density profiles of dephosphorylated and phosphorylated NF pairs for both interfilament separations.

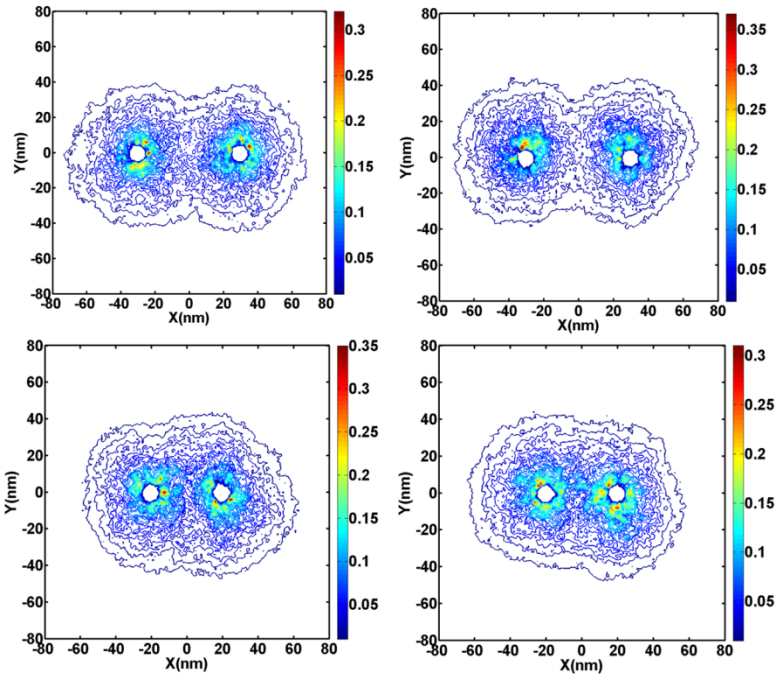


**Fig. 3.6** Two-dimensional contour plots of the average cross-sectional density profile $\rho(x, y)$ of the 60-nm apart dephosphorylated (**a**) and phosphorylated (**b**) NF pair under ionic conditions. Similar contour plots of $\rho(x, y)$ for the 40-nm-apart dephosphorylated (**c**) and phosphorylated (**d**) NF pair at 150 mM ionic concentration

An interesting observation from the contour plots depicted in Fig. 3.6 is that the monomer densities are significantly concentrated around the core of each filament (refer to the scale). Even at 40 nm separations, where a relatively higher overlap is observed under physiological condition, the central region between the cores shows only a fraction of the overall density profile. Clearly, the cylindrical geometry allows the sidearms to surround the curvature of the backbone in an effort to retract from the apposing sidearms. A similar behavior was reported by a study that investigated the polymer-mediated interactions between nanorods (Frishchknecht 2008). In this report, the polymeric chains that are end tethered to the cylindrical rods escape from the central narrow region to surround the curvature, decreasing the force between approaching structures. This

observation points to the importance of proper geometry in accessing available configurational space that relieves steric repulsion between monomers from adjacent filaments.

In general, the average density profile of apposing sidearms under salt free condition reveals no significant overlapping or interpenetration, suggesting a repulsive type of interactions under this condition. In contrast, under physiological condition, the electrostatic interaction observed in the salt-free condition is screened by the presence of salt ions, leading to a short-range steric exclusion type of interaction. Furthermore, when the proximity between the NF cores is changed from 60 nm to 40 nm, the monomers in each sidearm rearrange themselves so as to relieve the local steric repulsions, adopting a conformation with relatively higher overlapping density profile.

*Mutual interpenetration of apposing sidearms*

The conformational properties discussed above reveal the mutually exclusive behavior of apposing sidearms in the salt-free conditions, while some level of overlapping or mutual interpenetration was observed at 150 mM ionic solution. To assess the level of interpenetration under physiological conditions, we defined a conformational measure that quantifies the degree of mutual interpenetration or overlapping probability as described below. Furthermore, to reveal the changes in the level of mutual interpenetration as the interfilament separation decreases, we performed MC simulations of NF pairs by gradually reducing the interfilament distance from 60 nm towards 40 nm. In this process, starting from the equilibrated configuration at 60 nm separations, each filament is displaced by 1.25 nm towards the opposing filament, resulting in a total reduction of 2.5 nm in interfilament separation. The NF pair was then fully equilibrated at the new separation before subsequent production runs are performed for data collection. At the same time, the last configuration from the equilibration stage was taken as the starting configuration for the following compression step. This process was repeated systematically to gradually reduce the interfilament

distance to 40 nm. The change in the overlapping probability arising from gradual compression of adjacent filaments was analyzed from the equilibrated data as detailed below.

*Overlapping probability*

To estimate the interpenetration between adjacent filaments, we defined an averaged quantity $I$ that measures the overlapping or interpenetration probability of apposing sidearms. For any given condition (interfilament separation, ionic strength, or phosphorylation states), we define $I$ as the probability of finding monomers from one filament in the opposite half side of the region between the two filaments. The opposite half side corresponds to the (intermediate) region between the backbones of the two filaments that is above the mid-point for the filament on the left and below the mid-point for the filament on the right.

Mathematically, this can be expressed as

$$I = \frac{\int_0^{R/2} \rho_2(x)\,dx + \int_{R/2}^{R} \rho_1(x)\,dx}{\int_0^{R} \rho(x)\,dx}, \tag{3.8}$$

Where, R is the interfilament separation. $\rho_j(x)$ is the number density of monomers from filament $j$ that are found in the region between $x$ and $x + dx$ at the intermediate region of the apposing filaments. Note that the x-axis is defined along the line joining the centers of the longitudinal axes of the filament cores. Conventionally, the longitudinal axes are selected along the z-axis, and hence the y-z plane bisects the line joining the centers of the longitudinal axes. $\rho_j(x)$ is thus calculated from the number of monomers with in a small volume bounded by the y-z planes bisecting the x-axis at $x$ and $x + dx$. The values obtained from numerically integrating $\rho_j(x)$adjacent to the opposite filament are then normalized by the total number of monomers that

are found in the region between the two filaments, i.e., those bounded by the $y-z$ planes at $x=0$ and $x=R$.

Figure 3.7 depicts the monomer density $\rho_j(x)$ of phosphorylated NF pairs for interfilament separations $R$= 40, 45, 50, 55 and 60 nm under physiological condition. The plot shows that the average density $\rho_j(x)$ of the sidearms is concentrated near the backbone and gradually decreases towards the opposite filament. The interpenetration of the sidearms in the central region is indicated by the overlapping monomer density profiles. As observed in the figure, the extent of overlap increases as the backbones are compressed towards each other. The overlap/interpenetration is quantified by the interpenetration probability$I$, which was calculated by numerically integrating $\rho_j(x)$ of each filament beyond the midpoint. The value of $I$ calculated from such analyses is then examined under different conditions.

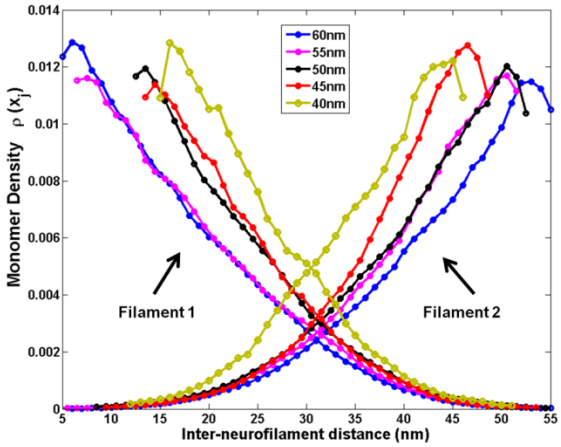


**Fig. 3.7** The average density $\rho\ j(x)$ of sidearm chain monomers as a function of the distance $x$ from the surface of each filament $j$ in a direction along the line normal to the filament axes. The plot shows the data for a 60, 55, 50, 45, and 40-nm-apart NF pair under physiological conditions

Figures 3.8(a-d) present the overlapping or interpenetration probability $I$ of adjacent NFs and the individual sidearms NFL, NFM and NFH respectively, under physiological conditions for different phosphorylation states and interfilament proximity. First, as expected, a monotonically increasing overlapping probability was observed as the interfilament distance is decreased (Fig. 3.8a). For example, the interpenetration probability for the 60 nm apart phosphorylated NFs is about $I = 0.07$, whereas nearly 50% increase in I was observed as the interfilament separation is reduced from 60 nm to 40 nm (i.e., $I = 0.14$ at 40 nm separations). Using planar grafted NF brush model, a similar monotonically increasing sidearm interpenetration behavior was observed by Stevens and Hoh as the opposing planar brushes are compressed towards each other (Stevens and Hoh 2011).

Among the three NF sidearms, NFL sidearms show the minimum overlapping probability, explained by their relatively shorter lengths (Fig. 3.8b) ($I \sim 0$ at 60 nm and increases exponentially to $I \sim 0.03$ as the interfilament distance decreases to 40 nm separations). In contrast, both NFM (Fig. 3.8c) and NFH (Fig. 3.8d) display relatively higher overlap probability at 60 nm, a value that increases in a weak exponential manner with decreasing interfilament separations. As shown in the figure, all data have been fitted to exponential functions, where the goodness of the fit was estimated based on the $R^2$ values are shown in the figure. In general, although a relative increase in overlapping probability was observed with a decrease in interfilament separations, compared to the number of monomers localized around or near the core of the backbone, the absolute number of overlapping or interpenetrating monomers is not large. Also, the difference in the overlapping behavior between phosphorylated and dephosphorylated states is not significant at the physiological condition.

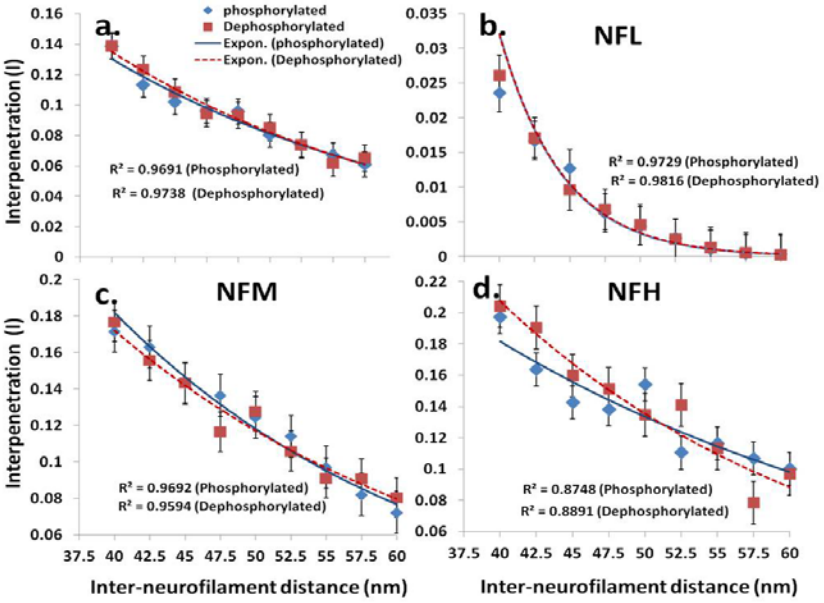


**Fig. 3.8** The overlapping or interpenetration probability (I) of an adjacent NF brush as a function of interfilament separation under physiological conditions. The plot (**a**) shows the overall mutual interpenetration probability of the adjacent NF brush. (**b**–**d**) represents I for individual sidearms NFL (**b**), NFM (**c**) and NFH (**d**) for dephosphorylated (▪) and phosphorylated (◆) states. The data were fitted by exponential functions and are shown by a *dashed line* (--) for dephosphorylated and a *solid line* (-) for phosphorylated systems. The goodness of the fit for individual data as estimated by the R2 value is shown in the figure. The error bar represents the standard error (SE) of the mean I value

*Average NF brush height*

Another useful quantity that captures the conformational behavior of NF sidearms is the height of the NF brush pair. The mean brush height $\langle x_j \rangle$ of a single filament $j$ is determined by taking the first moment of monomer distribution as

$$\langle x_j \rangle = \frac{\int x_j \rho(x_j)}{\int \rho(x_j)} \tag{3.9}$$

Where, $\rho(x_j)$is the number density of monomers in a small volume $dV(\equiv dxL_yL_z)$ at a distance $x_j$ form the core of the filament $j$, in a direction towards the adjacent filament. Note again that the $z$-

direction is along the longitudinal axis of the NF core, and the brush height is measured in the $x$-direction. Since we are interested in the brush height of the opposing filaments as they are facing each other, $\langle x_j \rangle$ is calculated based on the number density of the NF brush in the region between the two filaments. The average brush height h of the two filaments is then calculated as: $h = \frac{\langle x_1 \rangle + \langle x_2 \rangle}{2}$.

Fig 3.9 depicts the average brush height $h$ of the two filaments as a function of the interfilament distance under both phosphorylation states. The figure shows that $h$ monotonically decreases from 13.5 nm for the 60 nm separations to 11 nm for 40 nm separations, undergoing approximately a 20% reduction in size when the filaments are compressed from 60 nm to 40 nm. In terms of individual sidearms, NFL does not show any particular pattern in its brush height, whereas both NFM and NFH sidearms mimic the pattern observed for the overall brush height (data not shown).

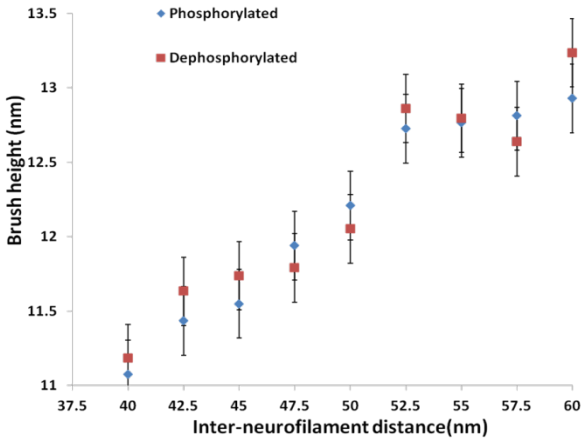


**Fig. 3.9** The average brush height "h" of the phosphorylated (◆) and dephosphorylated (■) NF brush as a function of interfilament separation under physiological condition. The error bar represents the standard error (SE) of the mean h value

Similar to the overlapping probability, under physiological condition, the difference between dephosphorylated and phosphorylated systems is not significant. These results demonstrate the tendency of the NF brush to adopt a collapsed conformation (as demonstrated by the decrease in brush height) as the adjacent filaments approach each other. Although the mutual interpenetration between the brushes increases as they approach each other, the present result clearly shows that NF brushes shrink in their height to retract themselves as the interfilament separation decreases.

*3.4. Discussion & Conclusion*

In our study, we investigated the conformational properties of a pair of interacting neurofilaments. These properties allow us to understand the nature of interacting neurofilaments and may shed light into the behavior of sidearm-mediated NF interactions. The structural reorganizations of interacting NF pairs were examined under various conditions. To this end, we performed MC simulations of a pair of NFs by using the sequence based coarse-grained NF brush model of Chang et al (Chang et al. 2009). The MC simulations were done under varying ionic condition, phosphorylation state, and interfilament separations.

To reveal the conformational properties of interacting NFs, we employed different complementary measures that capture the behavior of interacting adjacent neurofilaments. Our analysis indicates that, under salt-free condition, apposing sidearms bend away from each other forming a depletion region, a region that becomes large with increasing interfilament separation, at the center of the opposing filaments. It is interesting to point out that, although the geometry is different, a similar behavior has been found in the experimental study of interacting spherical polyelectrolyte brushes (SPBs) (Fig. 3.10a) (Wittemann et al. 2005). By using cryo-TEM experiments, Wittemann et al. demonstrated that, under low ionic strength, the chains of the brush layers in two opposing SPBs bend away when the SPBs are close to each other (Wittemann et al.

2005). This low ionic strength behavior of SPBs resembles the observation in the salt-free condition of the present study (Fig. 3.10a), except for the additional polyampholytic nature of the NF system.

To assess the conformations of interacting NF pairs under physiological condition, we performed a set of MC simulations under 150 mM ionic solutions. The results from these simulations reveal significant conformational changes when compared to the salt-free condition. Under ionic solution, the sidearms are found to adopt a coiled conformation in both phosphorylation states. A similar transition from a stretched to coiled conformation has been observed experimentally for the interacting SBPs mentioned above (Wittemann et al. 2005). The authors demonstrated that the polyelectrolyte chains are strongly stretched under low ionic strength and assume a coiled conformation under high ionic strength, i.e., in the limit of the salted brush.

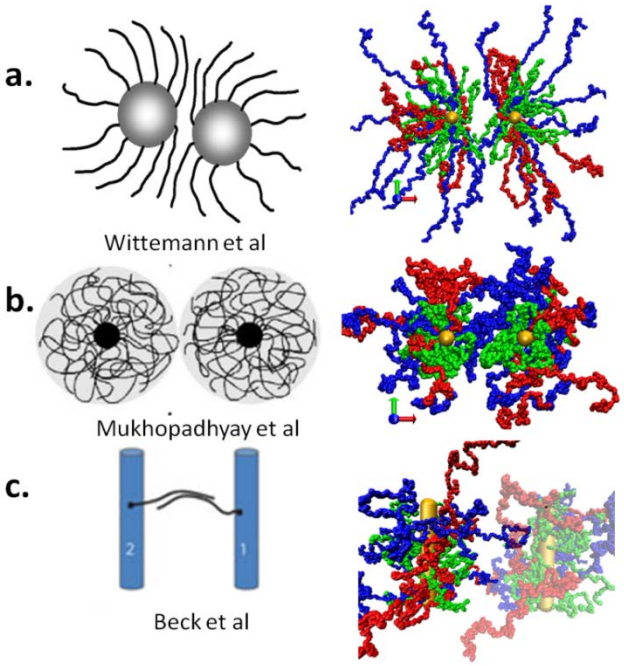


Fig. 3.10. Comparison of proposed models in the literature to the present study: **a** Interactions of spherical polymeric brush (SPBs) at low-ionic strength (Wittemnann et al. (Wittemann, 2005 #95) compared to the representative snapshot from the present MC simulation. The snapshot shows 40-nm-apart phosphorylated NF brush pair under salt-free condition. The schematic depiction on the left-hand side was adapted with permission from: Wittemann, A., M. Drechsler, et al. (2005). J. Am. Chem. Soc. 127(27): 9688–9689 Copyright@2005 American Chemical society . **b** A schematic representation of the entropic brush model that was proposed by Brown and Hoh (Brown and Hoh 1997) as reviewed by Mukhopadhyay et al. (Mukhopadhyay et al. 2004) vs. a snapshot of 40-nm-apart phosphorylated NF brush pair under 150 mM of ionic solution. The schematic representation on the left-hand side was adapted from: Mukhopadhyay, R., S. Kumar, et al. (2004). Bioessays 26(9): 1017–1025. With permission from Wiley Interscience **c.** The 'handshake' sidearm interaction model proposed by Beck et al. (Beck et al. 2012) vs. a side view for representative snapshot of 40-nm-apart phosphorylated NF brush pair under 150 mM ionic strength. The schematic depiction on the left-hand side was adapted from Beck, R., J. Deek, et al. (2010). Nat. Mater. 9(1): 40–46 . with permission from Nature.

The change from the stretched, mutually excluding bent conformations to the coiled, interpenetrating conformations suggests a change in the nature and type of interfilament interactions under ionic solution. In this regard, different mechanisms have been proposed to describe the interaction between neurofilaments. Based on the observation that NF sidearms are abundant with ionizable amino acid residues, sidearm-mediated interfilament interaction is described in terms of repulsive electrostatic interaction (Carden et al. 1987). In particular, the net negative charges attained from serine phosphorylation of the KSP repeat motifs were considered to be responsible for sidearm-mediated NF interaction (Carden et al. 1987, Dewaegh et al. 1992). The mutually exclusive type of conformations observed in the present study suggests apposing sidearms interact through electrostatic repulsive interactions under salt free condition.

Under 150 mM ionic solutions, the apposing sidearms were found in a coiled conformation. Clearly, this is the effect of the ionic screening. The electrostatic interaction would be short ranged since the Debye screening length is ~ 1 nm in 150 mM monovalent ionic solution. Therefore, from the observed coiled conformation, it would be reasonable to argue that repulsive type of interaction is not a likely mechanism for NF-NF interactions under physiological ionic concentration. A similar conclusion was drawn by Brown & Hoh (Brown and Hoh 1997) based on the atomic force microscopy measurement of isolated NFs in the presence of co-isolating contaminants.

The experiment revealed the exclusion of co-assembled material from the proximity of the NF core and the presence of weak repulsive forces that extend for more than 50 nm from the filament core (Brown and Hoh 1997). The authors then argued that such repulsion cannot be explained solely by electrostatic interaction that has a much shorter range due to the ionic screening (Brown and Hoh 1997). They predicted thermally driven motion of sidearms results in an entropic brush and is responsible for regulating the interfilament spacing (Brown and Hoh 1997). Others have argued interfilament interactions to be governed by the cross-bridge formation

between adjacent filaments (Hirokawa 1982, Hirokawa et al. 1984, Letterier 1987, Leterrier et al. 1996).

In the cross-bridge model, the non-covalent binding of NF sidearms, either by themselves or mediated by other accessory agents, is considered to be responsible for NF interactions. This hypothesis was originally based on electron microscopy (EM) studies of the frog axon where sidearms were found to form a dense network of cross-bridges that were 4-6 nm in diameter and 20-50 nm in length (Hirokawa 1982). Some authors questioned these results by describing the cross-bridges as "artifacts" arising from the EM methods (Price et al. 1988, Mukhopadhyay et al. 2004), but a recent study by Beck et al. (Beck et al. 2010) supported cross-bridge interaction. The authors studied NF gels under varying pressure and revealed that NF gels undergo an abrupt transition from the gel expanded to the gel condensed state under high osmotic pressure. Noting the irreversibility of the gel-condensed state, the authors argued for an attractive interaction to overcome the repulsive interaction dominating the gel expanded state (Beck et al. 2010). Then, they predicted NFs interact via attractive ionic cross-bridging of the polyampholyte sidearms in a 'handshaking' manner (cf. Fig. 3.10c).

In reference to cross-bridge interactions, our conformational analysis revealed monotonically increasing overlapping probability (under ionic solutions) as the adjacent neurofilaments are compressed from 60 nm to 40 nm separations. However, from the snapshots and the average properties like density profile (cf. Fig. 3.4 - 5), the overlapping between the apposing sidearms does not appear to be in a 'hand-shake' manner as depicted in the cross-bridging model (Gou et al. 1998, Beck et al. 2012 ). Refer to Figs. 3.10b and 3.10c for comparison between proposed models of interacting NFs found in the literature (left panels) and snapshots of NF pairs from the MC simulations (right panel). Nonetheless, it is interesting to point out that the density profiles shown in our study exhibit close similarity to the conceptual drawings shown in Fig. 3(e,f)

of Beck et al., (Beck et al. 2012) which were drawn to describe sidearm interactions under different compression levels.

It is important to emphasize that, in spite of the increase in the overlapping probability *I* as the interfilament distance is reduced from 60 nm to 40 nm, the absolute value of *I* is not significantly large (cf. Fig. 3.8a). From these observations, it is fair to speculate that the likelihood of cross-bridge interaction as the dominant mechanism for sidearm-mediated NF interaction is small. Instead, as proposed by Brown et al. (Brown and Hoh 1997), the conformational properties observed in our study suggest the entropic interaction as a likely mechanism for sidearm-mediated interactions under physiological conditions. In conclusion, the study of equilibrated NF pair conformations under different conditions reveals opposing sidearms from adjacent filaments do not interdigitate under salt-free condition, but rather bend away from each other forming a depletion region at the center. This suggests that the repulsive electrostatic interaction would be the dominant interaction for apposing sidearms under salt-free condition. At the physiological salt concentration, opposing sidearms exhibit coiled conformations with increasing overlapping upon compression, suggesting that entropic type of interaction may be dominant under physiological condition.

## Chapter IV

## Effect of hydrophobic interactions and $Ca^{2+}$ on the structure of neurofilament brush

This work was published in Kim et al. 2011.

### *4.1. Introduction*

The conformational properties of C-terminal domains exert a key influence on the NF architecture and function. Therefore, a study of the detailed nature of sidearms under different physiological conditions is essential for comprehensive understanding of NF biology. In lieu of the polyampholytic nature, the morphological characteristics of NFs are sensitive to variations in physiological parameters, especially, ionic strength, pH and divalent ions. Previous studies have examined the effect of monovalent ionic concentration (~150 mM) and phosphorylation on the conformational changes of the human and mouse NF architecture (Chang et al. 2009; Stevenson et al. 2011). These studies were instrumental in revealing the transient nature of NF sidearms and the NF brush structure in response to changing phosphorylation and ionic strength conditions (Chang et al. 2009; Stevenson et al. 2011, Lee et al. 2013).

Another related issue corresponds to the effect of divalent ions on the structure of NF sidearms. A recent experimental study by Lin et al. (Lin et al. 2010), examined the elastic properties of NFs in the presence of divalent ions. The results revealed that the divalent ions ($Mg^{2+}$) (1-10 mM) act as effective cross-linkers between adjacent filaments. Similar results were also reported by other experimental studies that provided evidence to the mediation of cross-bridges by multivalent ions such as $Al^{3+}$ and $Ca^{2+}$ (0.5 mM) (Kushkuley et al. 2010). It is hypothesized that the multivalent ions screen the repulsive interactions between charged residues on the sidearms leading to their collapsed conformation, and induced a cross-bridge type of interaction between the adjacent filaments (Letterier 1987; Leterrier et al. 1996; Kumar et al. 2002). In view of this, further study on

the effect of multivalent ions on the structure of NF sidearms is necessary to gain further insight into the NF organization.

In our study, under aim II we examined the effect of $Ca^{2+}$ on the structure of NF at varying ionic concentration and phosphorylation conditions. The effect of $Ca^{2+}$ is of relevance to neurofilament compaction, an event that occurs during axonal injury, as this pathology involves an influx of $Ca^{2+}$ into the axoplasm (Povlishock and Christman 1995, Buki and Povlishock 2006). An interesting question in this regards is : what is the influence of $Ca^{2+}$ ions on the organization of NF sidearms? The increase in the intra-axonal $Ca^{2+}$ concentration has been linked to the disruption of NF sidearm interactions that in turn leads to NF compaction. In spite of a general understanding on the occurrence of NF compaction upon excessive $Ca^{2+}$ influx, the pathogenesis of the initiating sub-cellular or molecular events remains unclear. Motivated by this, we carried out MC simulations of the NF brush under the influence of varying concentrations of $Ca^{2+}$ and monovalent salt, under both phosphorylation conditions. These results are expected to enhance the current understanding of the effect of divalent ($Ca^{2+}$) ions on the NF structure under varying ionic conditions.

In addition to the charged residues, the sidearms are also rich in hydrophobic residues. Fig. 4.1. depicts the distribution of hydrophobic amino acids, of the three sidearms NFL, NFM and NFH. Each point corresponds to the number of hydrophobic residues out of 30 amino acid residues. Regardless of the NF sidearm type, the hydrophobic sites are evenly distributed along the polypeptide chain, consisting of about 28 % (NFL) or 35 % (NFM and NFH) of total amino acid residues. Although, electrostatic interactions and entropic repulsion are expected to dominate the lateral extension of NF sidearms, it would be interesting to explore the effect of hydrophobic interaction in modifying the radial extension of the sidearms.

Up to this point, for all NF systems investigated the hydrophobic interaction was not considered, only focusing on the electrostatic correlation between amino acid residues. In the study under aim II, we examined the effect of hydrophobic interactions on the NF architecture by employing a simplified square well-potential for the hydrophobic interaction. Such an approach has been utilized in the past to study the polyelectrolyte systems (Chervanyov and Heinrich 2009; Cherstvy 2011). This method provides a computationally manageable technique to study the effect of hydrophobicity on our system. The results in this study in combination with our previous studies provide a comprehensive understanding of the properties of single human NF brush system under different phosphorylation and physiological conditions.

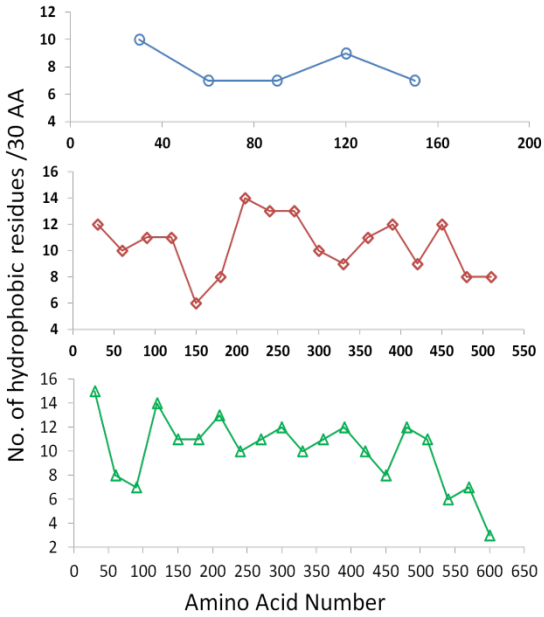


Fig. 4.1. The distribution of hydrophobic amino acid residues along each NF sidearm (NFL (blue), M (red) and H(green)). Each point corresponds to the number of hydrophobic amino acid residues out of 30 amino acid residues.

*4.2. Methods*

The sequence-based coarse-grained 3D NF brush model that was employed for Specific Aim I was adapted to include the effect of hydrophobic interactions and divalent ions. In this study, the model consists of a single NF brush in which the backbone is modeled as an infinitely long rod of diameter $\sigma_B$ = 10 nm, with sidearms tethered to it. The rod is centered at the origin of the simulation box of dimensions 200 x 200 x 50 nm. Similar to the previous human NF brush model, a total of 31 sidearms were tethered in the ratio of NFL: NFM: NFH of 7:3:2 of human NF. Accordingly, 18 NFL: 8

NFM:5 NFH were grafted. The sidearms are tethered around the core in an equally spaced but randomly grafted around the core of the filament. While in the original model the interaction potential is represented as the sum of hard-sphere and electrostatic interactions, in the present model, it is calculated as the sum of excluded-volume, hydrophobic and electrostatic interactions. Both the excluded-volume and hydrophobic interactions between CG sites are represented by a square-well potential, $U_{well}$ that is defined as

$$U_{well} = \begin{cases} \infty & \text{when } r_{ij} < \sigma_s \\ -\lambda\epsilon_{ij} & \text{when } \sigma_s \leq r_{ij} < 2\sigma_s \\ 0 & \text{otherwise} \end{cases} \quad \cdots (4.1)$$

Where, $r_{ij}$ is the distance between the centers of two CG sites i and j, and $\sigma_s$ is the diameter of the CG site and is set to 0.6 nm, following our previous studies (Chang et al. 2009; Stevenson et al. 2011). $\epsilon_{ij}$ is the well-depth of the hydrophobic interaction between i and j residues given by $\epsilon_{ij} = \sqrt{\epsilon_i \epsilon_j}$ . According to Zhulina and Leermakers, (Zhulina and Leermakers 2007) the hydrophobic interaction well-depth, $\epsilon_i$ of amino-acid residue $i$ is set to 2.0 $k_B T$ ($k_B$ is Boltzmann constant and T is absolute temperature) for hydrophobic (apolar) residues (glycine, proline, cysteine, methionine, alanine, leucine, valine, and isoleucine), 0.6 $k_B T$ for polar residues (tyrosine, glutamine, histidine, phenylalanine, and tryptophan), and 0 for the rest. However, this set of parameters tends to drive the neurofilament system into strongly trapped states at local minima. To allow variation in the strength of hydrophobic interaction and assess the conformational changes arising from such interactions, we introduced a hydrophobic scaling factor λ, which ranges from 0 to 1, to control the hydrophobic interaction between CG sites. Such a range allows us to explore the contribution of hydrophobic interactions in the lateral extension of sidearms.

Similar to the original model, the electrostatic interactions are represented by a mean field screened coulomb interaction, $U_{el}$, where both solvents and monovalent ions such as $K^+$ and $Cl^-$ ions are implicitly incorporated into the electrostatic potential energy (refer to equation 3.4 of the methods section in Specific Aim 1). However, since the screened Coulomb potential approximation

breaks down for multivalent ions, the divalent salt ions needed to assess the role of $Ca^{2+}$ in affecting sidearm conformations are incorporated in the model explicitly. The effect of calcium ions has been investigated by choosing the concentration in the range of [$Ca^{2+}$] = 0 mM to 0.8 mM in the presence of monovalent ionic salts I = 1, 10 and 100mM under dephosphorylated and phosphorylated conditions.

The interaction between the NF backbone and sidearm residues is approximated by hard sphere type potential, $U_{hard}$, defined as

$$U_{hard} = \begin{cases} \infty & when\ r_i < \dfrac{\sigma_B + \sigma_s}{2} \\ 0 & otherwise \end{cases} \qquad \cdots (4.2.)$$

where, $r_i$ is the distance between the CG site $i$ and the NF backbone core. The sidearm chains are subject to additional bonding potentials for bonded pairs, the bond length of which is fixed to $\sigma_s$, but do not have any angle or dihedral potentials. Therefore, each NF sidearm is represented as a freely-jointed chain with monomer diameter $\sigma_s$.

*Simulation techniques*

We followed the simulations techniques as described in the previous section (Refer to "Simulation methods" of specific aim I, section 3.2 for a detailed description). Similarly, the initial configurations were generated and the standard MC simulations were then performed to equilibrate the system under each condition, until the system energy and the size of sidearm chains as measured by the radius of gyration stop from drifting. Starting with each of the equilibrated configurations, the configurations of sidearms are sampled using the MC simulations, and saved every 1000 - 5000 moves. Equilibrium properties such as monomer concentration profile and radius of gyration are then calculated from sampled configurations, the size of which is 1000 per each system. The reported value in this study is the average of at least 8 independent NF sidearm-tethered configurations for each condition, and the error represents one standard deviation obtained from the averages of the 8 independent simulations.

The structural properties of the NF sidearms are studied using simulation snapshots as well as statistical quantities such as radius of gyration and lateral concentration profiles. The radius of gyration Rg is defined as:

$$R_g = \sqrt{2R_{g\perp}^2 + R_{g\parallel}^2} \qquad \cdots (4.3)$$

$$R_{g\perp} = \sqrt{\langle \frac{1}{4N_S^2} \sum_{i,j}^{N_s} \left\{ \left(x_i - x_j\right)^2 + \left(y_i - y_j\right)^2 \right\} \rangle} \qquad \cdots (4.3.1)$$

$$R_{g\parallel} = \sqrt{\langle \frac{1}{2N_S^2} \sum_{i,j}^{N_s} \left\{ \left(z_i - z_j\right)^2 \right\} \rangle} \qquad \cdots (4.3.2)$$

where, Ns is the number of amino acid residues in each sidearm, $(x_i, y_i, z_i)$ is the coordinate of the residue site $i$, and indicates the ensemble average $\langle \dots \dots \rangle$. In addition, $R_{g\perp}$ and $R_{g\parallel}$ represent the components of $R_g$ in the directions perpendicular and parallel to the NF backbone axis, respectively.

On the other hand, the lateral concentration profile, $\rho(r)$, is defined as

$$\rho(r) = \frac{1}{2\pi r L_z} \sum_{i}^{N_s} \langle \delta(r - r_i) \rangle \qquad \cdots (4.4)$$

where, $\delta(\dots \dots)$is the Dirac delta function, $r_i$ is the distance between the residue site i and the NF backbone, and $L_z$ is the simulation box size in the z direction, which is 50 nm.

*4.3 Results*

*Effects of $Ca^{2+}$ ions on NF architecture*

Under Aim II, to understand the effect of $Ca^{2+}$ on the morphology of NF we carried out MC simulations of isolated NF brush in the presence of $Ca^{2+}$ ions, under phosphorylated and dephosphorylated conditions for various conditions of ionic strength. Figs. 4.2(a-c) present snapshots of the equilibrium structures of both phosphorylated and dephosphorylated NF in the presence of $[Ca^{2+}]$ = 0.4 mM and I = 1, 10, and 100 mM. As seen in the figure, the overall structure of dephosphorylated NF adapts a compact and denser conformation in the presence of $Ca^{2+}$. On the other hand, the phosphorylated NF appears to be relatively swollen, but with reduced overall radial extension. In terms of individual NF sidearms, the relative collapse in the flower-like extended architecture of the dephosphorylated NF results from the reduction or shrinkage in the radial stretching of both NFL and NFM sidearms. On the other hand, dephosphorylated NFH sidearms do not seem to be affected significantly (recall that NFH sidearms already have a collapsed conformation in the $Ca^{2+}$-free dephosphorylated state). With regard to phosphorylated sidearms, the radial extension of each sidearm is found to be reduced by some amount, the extent of which is described below.

To quantify the changes observed in the snapshots and determine the average behavior of $Ca^{2+}$-induced NF reorganization, the average radius of gyration and monomer density profiles have been measured. Figures 4.3(a-c) present the radius of gyration, *Rg*, of phosphorylated and dephosphorylated NF sidearms in the presence of $Ca^{2+}$ ions for various conditions of ionic strength. The figures compare *Rg* of NF sidearms at two different $Ca^{2+}$ concentrations, $[Ca^{2+}]$ = 0.4 and 0.8 mM, and without $Ca^{2+}$ (i.e 0 mM) at three different ionic concentrations (I = 1,10 and 100mM).

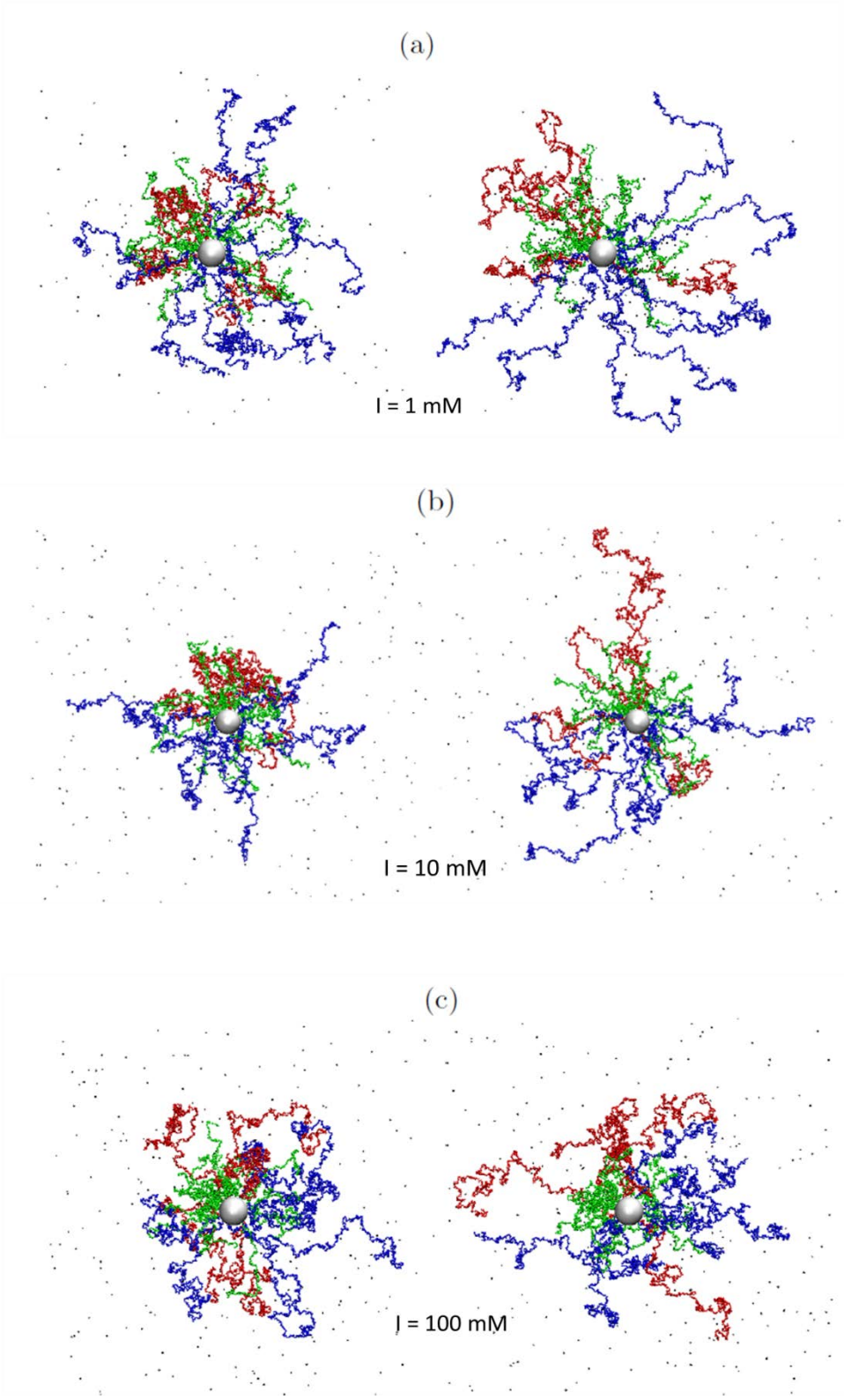


Fig. 4.2. Representative snapshots of the NF system at [$Ca^{2+}$] = 0.4 mM and *I* = (a) 1 mM, (b) 10 mM, and (c) 100 mM when it is both dephosphorylated (left) and fully phosphorylated (right). Different colors are assigned to each of the three types of NF sidearms: NFL (green), NFM (blue), and NFH (red), and $Ca^{2+}$ is represented as a black dot.

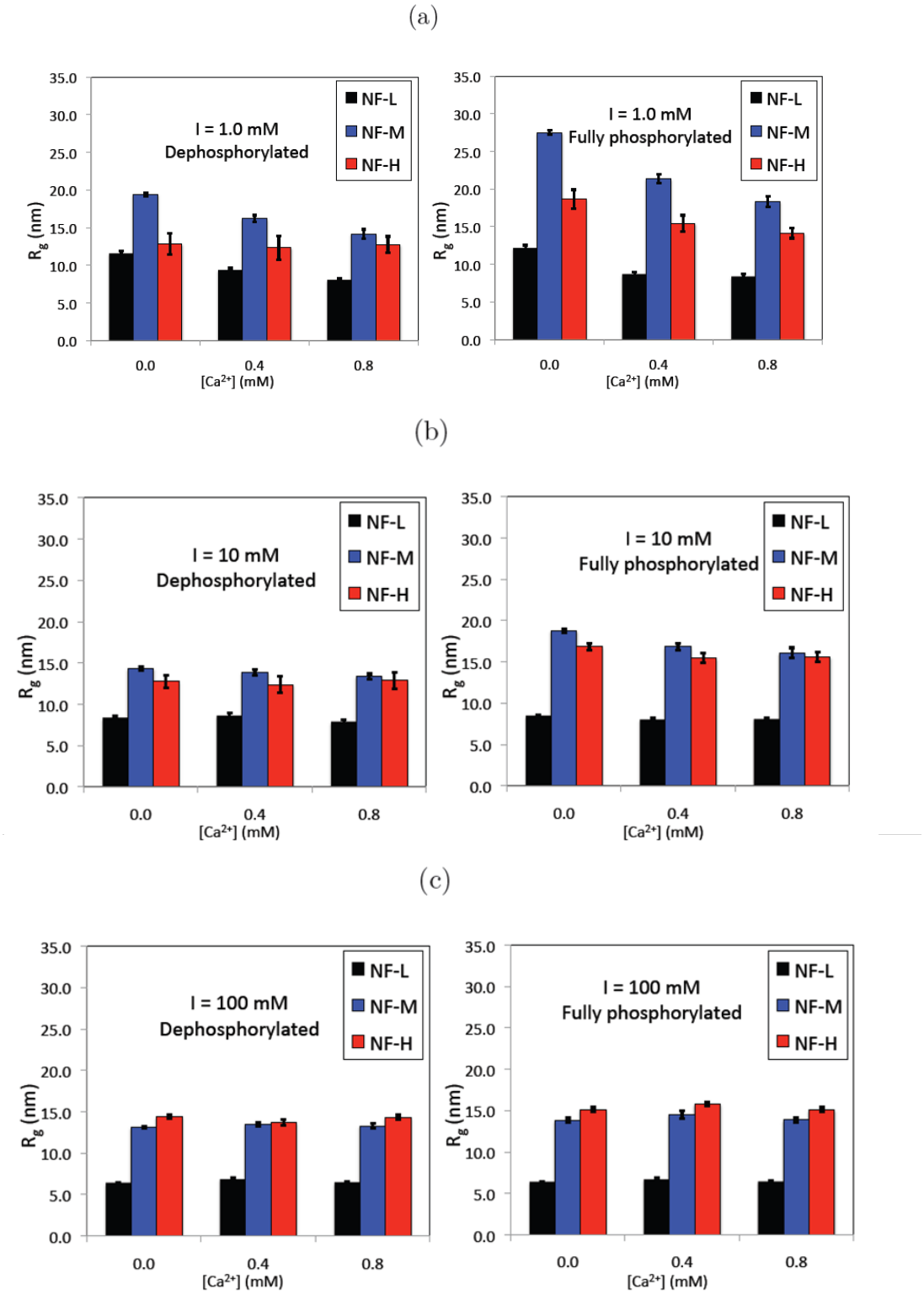


Fig. 4.3. Radius of gyration, *Rg*, of each sidearm as a function of ionic strength in the presence of $Ca^{2+}$ for both dephosphorylated (left) and fully phosphorylated (right) states when *I* = (a) 1 mM, (b) 10 mM, and (c) 100 mM, respectively.

Interestingly, at low salt concentration ($I$ = 1.0 mM) the presence of $Ca^{2+}$ ions significantly reduces the extension of dephosphorylated NFM sidearms, where *Rg* of NFM reduces from about 19.4 nm to 16.2 nm and 14.2 nm at [$Ca^{2+}$] = 0.4 and 0.8 mM, respectively. A similar decreasing pattern has also been observed in the dephosphorylated NFL subunit, albeit by a small amount. In contrast, *Rg* of dephosphorylated NFH exhibits little change or even a slight increase in the presence of $Ca^{2+}$ ions. At medium and high salt concentrations ($I$ = 10–100 mM), the extension of the NF sidearms is less sensitive because they are already significantly contracted at these high ionic strengths. With regard to phosphorylated NF sidearms, *Rg* of the three subunits are found to be smaller than those in the $Ca^{2+}$- free condition. Especially, phophorylated NFM sidearms that have the largest lateral extension in the $Ca^{2+}$-free condition exhibits a significant reduction in the presence of $Ca^{2+}$ ions, where *Rg* reduces from about 27.5 nm in the absence of $Ca^{2+}$ to 21.3 nm (for [$Ca^{2+}$] = 0.4 mM) and 18.3 nm (for [$Ca^{2+}$] = 0.8 mM) at dilute salt concentration ($I$ = 1 mM). The significant change of *Rg* in both phosphorylated and dephosphorylated NFM sidearms (to a lesser extent in NFL and NFH) suggests that $Ca^{2+}$ influences the local repulsive electrostatic interactions through the screening of charges on the polyelectrolyte sidearms at low ionic strength. The compaction of charged chains due to multivalent counterions such as $Ca^{2+}$ ions is well known in polyelectrolyte systems and has been attributed to a strong bridging-type correlation between charged monomers of the chains, mediated by multivalent counterions. (Dubois and Boue 2001, Zhang et al. 2001, Chang and Yethiraj 2003).

The above observations that are based on *Rg* can be supplemented by the lateral concentration profile, $\rho(r)$, of individual sidearms. Figures 4.4(a-d) present the results of this analysis, where the figures compare the density profile of individual sidearms both in the presence and absence of $Ca^{2+}$ ions at low and high salt concentrations. Figure 4.4(a) shows $Ca^{2+}$-dependent

changes of dephosphorylated sidearms at I=1mM. There is only a small change in the density profile of dephosphorylated NFH at low ionic strength ($I$ = 1 mM), where a slight decrease is found within the intermediate region. This $Ca^{2+}$-induced change of the NFH sidearm corresponds to a longitudinal (along the length of the filament) increase of the protrusion as opposed to a radially outward expansion. This can be seen by noting that the position at which the concentration profile drops sharply to zero is at about the same cutoff distance both in the presence and absence of $Ca^{2+}$ ions, suggesting that $Ca^{2+}$ ions do not have much effect in modulating the radial stretching of dephosphorylated NFH sidearms. The changes in dephosphorylated NFL are also small, where the cutoff distance at which the monomer concentration of NFL goes to zero is nearly the same both in the presence and absence of $Ca^{2+}$ ions. Therefore, in terms of the radial stretching, $Ca^{2+}$ ions appear to have an insignificant effect on both dephosphorylated NFH and NFL sidearms. However, a significant reduction has been observed in the cutoff distance of NFM (from ~75 nm in the $Ca^{2+}$-free structure to ~65 nm at $[Ca^{2+}]$ = 0.4 mM), pointing towards a significant compaction of dephosphorylated NFM sidearms in the presence of $Ca^{2+}$ ions. Figure 4.4. (b) presents the structural change of phosphorylated sidearms in the presence of $Ca^{2+}$ ions at $I$ = 1 mM. As shown in the figure, the phosphorylated NFL exhibits a negligible change in its density profile. However, unlike its dephosphorylated counterpart, the cutoff distance at which phosphorylated NFH drops to zero is significantly different. It changes from ~75 nm in the absence of $Ca^{2+}$ ions to ~65 nm in the presence of $Ca^{2+}$ ions. A similar behavior is observed for phosphorylated NFM sidearms, where the cutoff distance is reduced from ~100 nm in the absence of $Ca^{2+}$ ions to ~80 nm in the presence of $Ca^{2+}$ ions at $I$ = 1 mM, suggesting that $Ca^{2+}$ ions have a significant effect in reducing the length of stretched NFM sidearms. On the other hand, the effects of $Ca^{2+}$ ions on the structure of the NF sidearms are less significant at high ionic strength regardless of the phosphorylation state, as shown in Figs. 4.4(c) and 4.4(d). This is due to the screening effect of high ionic concentration. This can be further recognized by examining the charge density profile $\rho(r)$ of the $Ca^{2+}$ ions. Under high

ionic concentration, the $Ca^{2+}$ ions are spread farther out to the region where the concentrations of the C-terminal tail monomers are negligible. This is indicative that the $Ca^{2+}$ ions have less influence on the NF sidearms under high ionic condition.

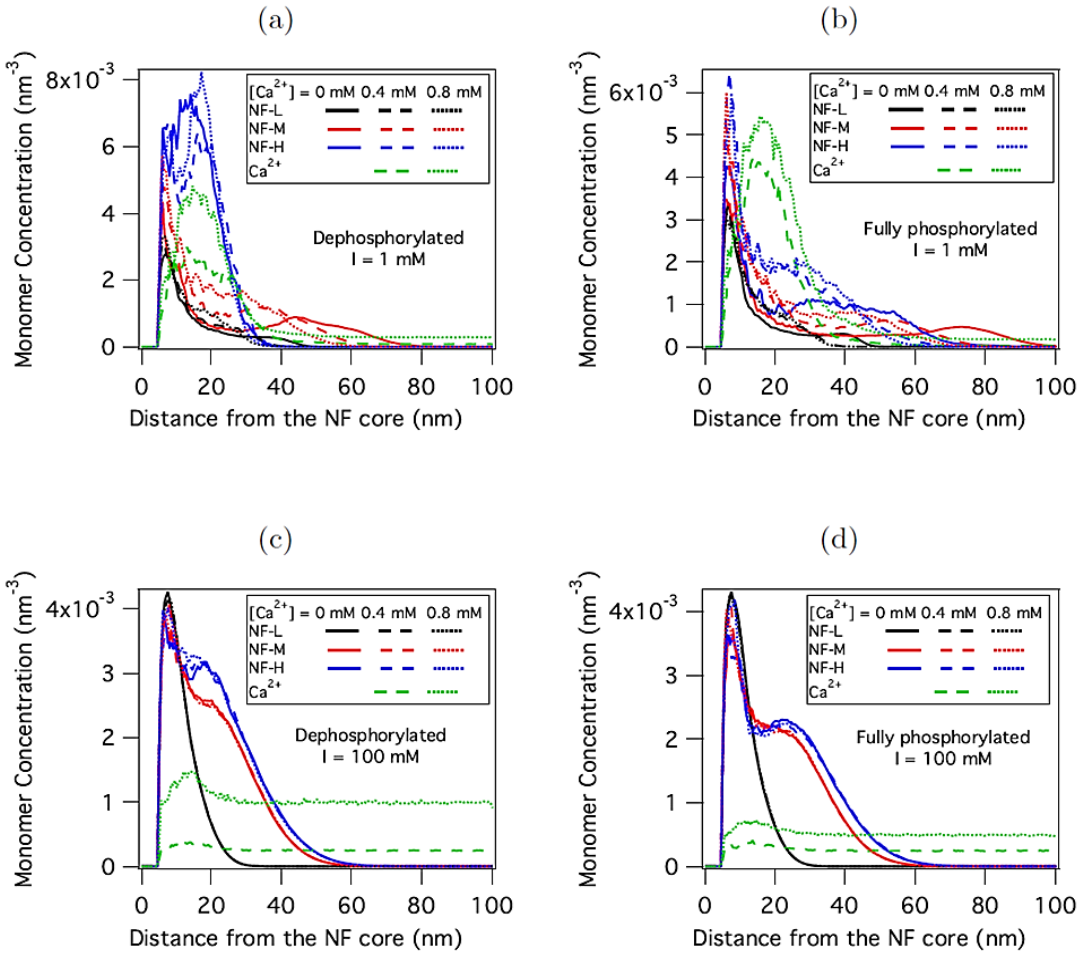


Fig. 4. 4. Lateral concentration profile, $\rho(r)$, of sidearm monomers and $Ca^{2+}$ ions as a function of the distance from the NF backbone in various ionic strength conditions of monovalent salt ions ($I$ = 1 and 100 mM) for both dephosphorylated ((a) and (c)) and fully phosphorylated ((b) and (d)) states.

This profile is in contrast with the charge density profile of $Ca^{2+}$ ions under low ionic strength. Under low ionic condition the $Ca^{2+}$ ions are localized near the filament core, a region where high density profiles of monomers are observed. Here, the $Ca^{2+}$ ions play the role of polyelectrolyte condensation and coil formation, influencing the lateral extension of sidearms.

*Effect of Hydrophobic Interaction*

Up to this point, for all NF systems investigated the hydrophobic interaction was not considered (i.e., $\lambda = 0$), only focusing on the electrostatic correlation between amino acid residues. However, as mentioned in the Introduction, the NF sidearms contain many hydrophobic apolar amino acid residues. Figure 4.1 displays the distribution of hydrophobic residues as a function of amino acid number across the length of NF C-terminals. One noticeable thing is that the hydrophobic sites are abundant throughout the chain, not localized at certain specific regions. Each point corresponds to the number of apolar residues out of 30 amino acid residues. Regardless of the NF sidearm type, the hydrophobic sites are evenly distributed along the polypeptide chain.

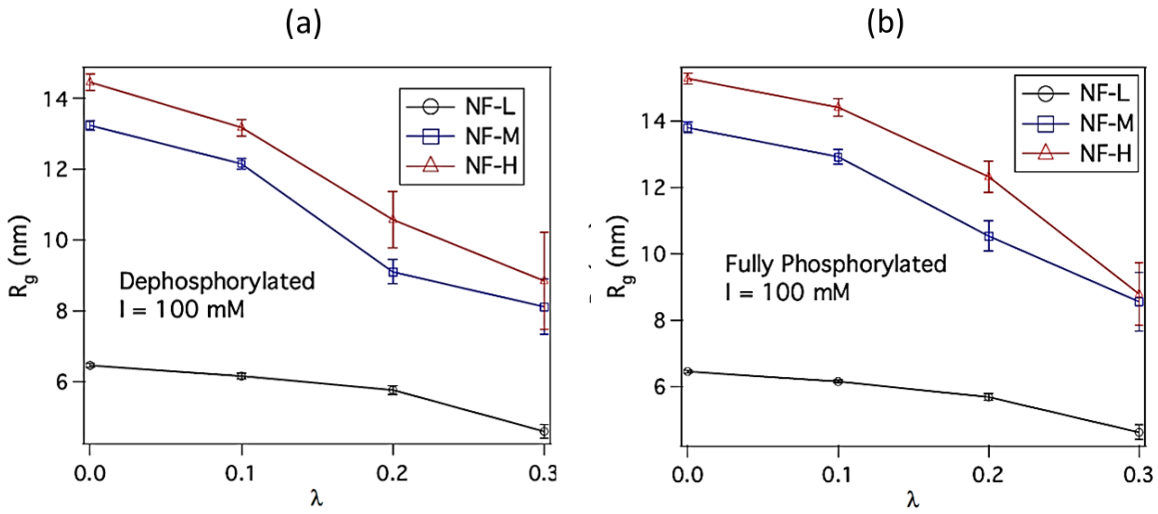


Fig. 4.5. Radius of gyration of each sidearm as a function of the hydrophobic interaction scaling factor, $\lambda$, at $I$ = 100 mM for (a) dephosphorylated and (b) fully phosphorylated states, respectively.

As mentioned in section 4.1., to examine the effect of hydrophobic interaction on the structural properties of the NF systems, squarewell potential was applied for hydrophobic residue pairs (see Eq. (4.1)). Though this approach allows us to address the effect of hydrophobic interaction in a computationally manageable manner, the use of well-depth in the square-well potential larger than $\lambda = 0.3$ tends to drive the NF system into locally trapped metastable states. To overcome this

challenge, we investigate the effects of the hydrophobic interaction by varying its strength, i.e., λ (between 0 and 0.3). Figures 4.5(a) and 4.5(b) show the radius of gyration, *Rg*, of each NF sidearm as a function of the extent of hydrophobic well-depth, $\lambda$, up to $\lambda$ = 0.3 at $I$ = 100 mM for dephosphorylated and fully phosphorylated states, respectively. As expected, as the hydrophobic interaction gets stronger (or $\lambda$ is increased), each NF sidearm becomes smaller. However, the relative extension among different types of sidearms does not change until $\lambda$ is as strong as 0.3, which implies that the hydrophobic interaction plays a role in the NF extension by diminishing the overall NF conformation rather than by inducing site-specific hydrophobic bridge formation.

*4.4 Conclusion*

In the present study our aim is to gain insight into the effect of divalent ions and hydrophobic interactions on the structural organization of isolated human neurofilament brush. We observe that the effect of $Ca^{2+}$ ions is prominent at low ionic concentrations (I = 1 mM, 10mM) as seen by reduction in the sidearm size ($R_g$) and monomer concentration profiles. The presence of $Ca^{2+}$ induces a collapse of the sidearms due to screening of electrostatic repulsions between charged residues. Whereas, at physiological concentration (I = 100 mM), the NF sidearms remain unaffected. The results of this study enhanced our current understanding of the effect divalent ions under the influence of varying ionic strengths on NF organization. It would be interesting to extend the present study to examine the effect of $Ca^{2+}$ ions on the NF-NF sidearm interactions to test the cross-linking effect of multivalent ions proposed by experimental studies. On the other hand, the introduction of hydrophobic interactions did not influence the structural organization except for reduction in the overall extension of the brush. However, it is to be noted that the present model does not take into consideration the hydrophobic interactions between the core and sidearms, which may have some effect on the conformational properties. The present study in combination with previous studies (Chang et al 2009, Stevenson et al 2011) on the isolated human NF brush

structure provided a comprehensive overview of the conformational properties of NFs under different physiological and non-physiological conditions.

# Chapter V

## Atomistic modeling of Medium Neurofilament (NFM) sidearm

### *5.1. Introduction*

NFs have a key role in establishing the axonal caliber of large diameter myelinated axons that determine the nerve conduction velocities**.** Trangenic mouse studies in the past decade have provided valuable insights into the role of individual subunits and their C-terminals in the NF function. Especially, studies involving C-terminal domains of NFM and NFH have concluded that NFM has a distinct role in specifying the axonal diameter (Rao et al. 2002; Rao et al. 2003). However, contrary to the existing hypothesis, the gene replacement study by Garcia et al on the phospho-incompetent mice, wherein, Serine in KSP was mutated Alanine, revealed that mutant mice the mutant mice exhibit comparable axonal growth in relation to wild-type (Garcia et al. 2009; Barry et al. 2012). Motivated by this unprecedented observation, our group examined the effect of phosphorylation on the mouse neurofilament using a sequence based coarse-grained approach (Stevenson et al. 2011). This study was carried out under three different phosphorylation conditions: dephosphorylated, phosphorylated and phospho-incompetent. The conformational properties of NF sidearms were examined in the presence and absence of physiological salt concentrations. The main observation of this study was that the lateral extension of NFM sidearms remains unaltered by KSP phosphorylation supported by the observations of Garcia et al.

While the 3D coarse grained models provide insights into the conformational properties of the sidearms, a deeper understanding of the intrinsic molecular changes, which govern the structure, holds the key to understanding the process of radial expansion by NFM. Molecular dynamics studies provide a valuable computational tool to study the ultra-structural changes of such complex biomolecules. This approach is helpful in revealing the dynamic behavior (time-evolved) behavior of macromolecules at an atomistic level, which may not be practical with experimental

methodologies. Briefly, the principle of MD is based on the Newton's second law of motion (Smit 2002). The atoms in a system are initialized with certain velocities, and the trajectories of these atoms are tracked by integrating Newton's equation on motion. The force between the interacting particles and the potential energy are defined by "force fields". The average properties of the system are then calculated as a function of time. Molecular mechanics packages include CHARMM, AMBER, NAMD and others. The advances in computational abilities have facilitated the application of MD to assess the biophysical properties of wide variety of macromolecular systems. Applications of the studies include DNA folding, protein-protein interactions and drug discovery etc (Scheraga et al. 2007, Kerrigan 2013, Jones et al. 2014). Recently, Lyons et al employed MD simulations to study the effect of phosphorylation induced conformational changes in microtubule associated protein tau (MATP) peptide under different phosphorylation and ionic strength conditions (Lyons et al. 2014). With regards to neurofilaments, Adiga et al. (Adiga et al. 2009) investigated the effect of phosphorylation on the conformation of NFH sidearm at different levels of phosphorylation. The results provided insightful details into the dominant inter-molecular interactions that govern the structure of NFH and their implications in NF transport.

Noting that NFM's are considered critical in their role of NF network, we attempt to investigate the conformational properties of NFM sidearm by employing atomistic modeling under different phosphorylation conditions. To this end, we carried out MD simulations of the mouse and mutated mouse (with 85 amino acids deleted) NFM sidearms under dephosphorylated, phosphorylated and phospho-incompetent conditions at physiological salt concentration (150 mM). To overcome the challenge of long structural relaxation times usually encountered with large biomolecules, we carried out our simulation using generalized born implicit solvent (GBSW) method that treats water as a dielectric continuum. The use of such implicit solvent model allows us to avoid the need for explicit modeling water molecules that is computationally expensive for extended polypeptide like NFM sidearms. Unfortunately, even the use of implicit solvent method

turned out to be extremely challenging for NFM sidearms, where we were unable to attain equilibrated conformation even after 30 ns of simulation times. As a result, the remaining discussion of this section presents the methods employed, the preliminary results and future direction of our effort on the subject.

*5.2. Method*

*Model*

In our study, we set out to gain insights into the structural changes at an atomistic level in the NFM sidearm brought about by KSP phosphorylation. To this end, we performed MD simulations on the atomistic model of NFM for the mouse and mutated mouse (NFM Δ with 85 amino acids deleted) under different conditions. The C-terminal sequence of mouse (438 aa) NFM were obtained from the Uniprot (UniProt Consortium. http://www.uniprot.org/uniprot.). The sequence for the NFM C-terminal tail of mutated mouse (360 aa) was provided by Dr. Michael Garcia's lab. The models for different phosphorylated states were setup using CHARMM facility. The force-fields for phosphorylated sequence was generated by applying the CHARMM inbuilt "patch" facility that adds phosphate group (SP2) to the serine-threonine motif. All simulations were carried out at 300 K temperature at standard physiological concentration (150 mM), using the generalized Born with simple smoothing functions (GBSW) implicit solvent model (Im et al. 2003, Chen et al. 2006) )as implemented in NAMD.

*Simulation methods and Data analysis*

We carried out MD simulations of NFM sidearms by using CHARMM force field parameters. For each simulation, the initial extended structure was first minimized using the steepest descent (SD) method and then briefly equilibrated at 300K for 50 ps. Then the MD simulations were continued to equilibrate the system until the total energy and average properties reach a mean value. As a measure for the equilibration of the polypeptide, we calculated the radius of gyration Rg of the NFM sidearms. Each of the simulations was performed at a time step of 2 fs and temperature of 300K for a total simulation time of 30 ns each. The trajectories obtained during these simulations were visualized using Visual Molecular Dynamics (VMD) and Rg was calculated using CHARMM analysis facility.

*5.3. Preliminary Results & Discussion*

The conformational changes in NFM were studied by performing MD simulations on the atomistic models of mouse and delta-mouse under different phosphorylation conditions. The time evolution of the structure was followed by calculating the energy and radius of gyration. Figure 5.1 shows the variation in total energy of dephosphorylated system under physiological conditions with respect to time. The radius of gyration $R_g$(upto ~31 ns) of the NFM structure in phosphorylated and dephosphorylated states is shown in Figure 5.2.

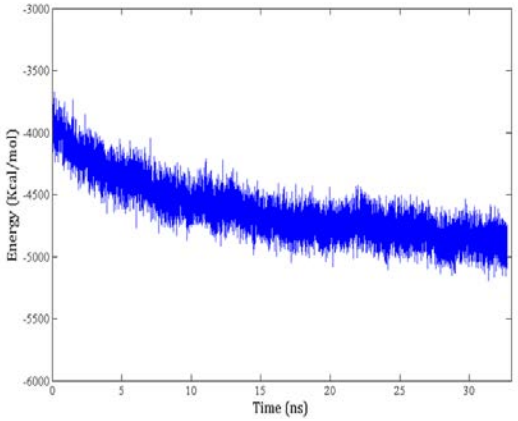


Fig. 5.1. Plot of total energy of dephosphorylated mouse NFM during MD simulation from completely extended

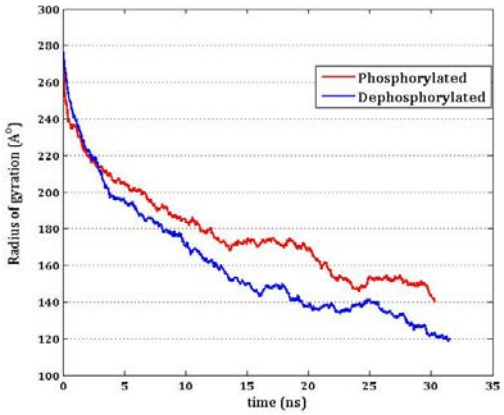


Fig. 5.2. Plots of Radius of gyration $R_g$ of phosphorylated (red) and dephosphorylated (blue) wild mouse NFM under physiological conditions during MD simulation.

As seen in the plots, at the present stage (31 ns simulation), the structures have not reached equilibrium, indicated by the tendency of energy and $R_g$ to decrease further. With regards to phosphorylation, a difference ~ 16 A° (or 1.6 nm) is noted with phosphorylated system having higher radius. In a previous study of the coarse-grained model of isolated NF brush, the $R_g$ of NFM at near physiological concentration (100 mM) were measured as ~ 12.2 and 12.6 nm for

dephosphorylated and phosphorylated systems respectively with a difference of ~0.4 nm (Stevenson et al. 2011). Based on the present trend it can be predicted that the difference in $R_g$ values between the two phosphorylated systems may decrease as the structures tend to stabilize.

VMD snapshots of mouse NFM in both phosphorylation states are shown in Fig. 5.3(a,b). In the phosphorylated structure the KSP repeats are represented by ball-stick model. With regards to conformational changes, in both phosphorylation states, the structure adapts an extended conformation. The **preliminary** results (both visual and quantitative) indicate that the structures exhibit minimal difference in their conformational changes with respect to phosphorylation which is in broad agreement with our previous studies on the NF brush (Garcia et al. 2009, Stevenson et al. 2011).

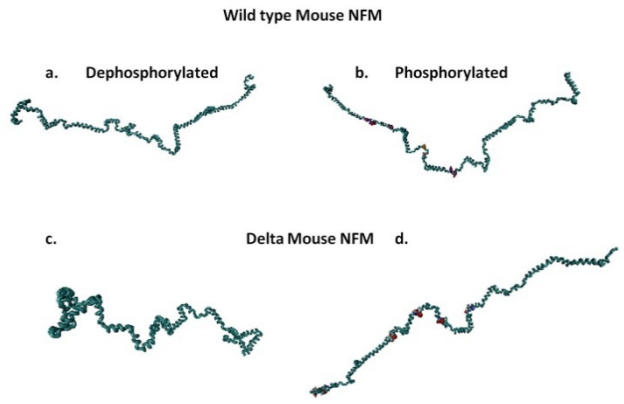


Fig. 5.3. VMD snapshots of Mouse NFM in a) dephosphorylated and b) phosphorylated states and Delta Mouse NFM in c) dephosphorylated and d) phosphorylated states at 30 ns. The KSP residues are represented in both phosphorylated systems are represented using ball and stick model.

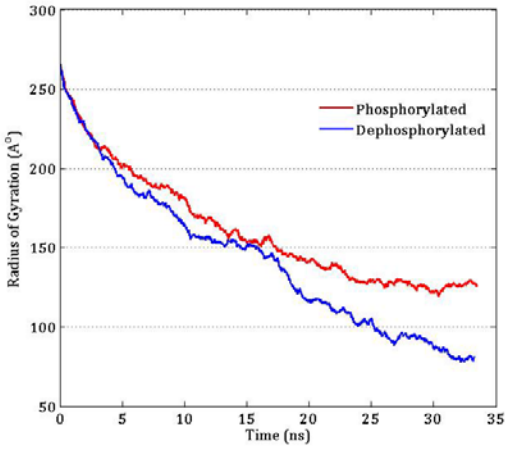


Fig. 5.4. Plots of Radius of gyration $R_g$ of phosphorylated (red) and dephosphorylated (blue) Δ mouse NFM under physiological conditions during MD simulation.

*Δ Mouse NFM*

Similar to NFM, MD simulations were also performed on Δ NFM, under different phosphorylation conditions. The initial part of the NFM C-terminal domain (upto 85 aminoacids) was deleted to generate ΔNFM, to examine the differential influence of the central part of the domain (containing

all the KSP repeats) versus wild type NFM, on NFM conformation. The sequence of ΔNFM is shown in Appendix I. Figure 5.4 shows the transition of $R_g$ with time in both phosphorylation states upto 32 ns. Similar to wild-type NFM a difference of ~ 15 A° (1.5 nm) is observed between the structures. Figure 5.3 (c, d) depict the VMD snapshots of ΔNFM in dephosphorylated and phosphorylated states respectively at 30 ns of simulation time. Visual analysis indicates that in a dephosphorylated state ΔNFM adapts a convoluted conformation with prominent loops when compared wild type NFM. On the other hand in the phosphorylated state, similar to wild - NFM, the structure adapts an extended conformation.

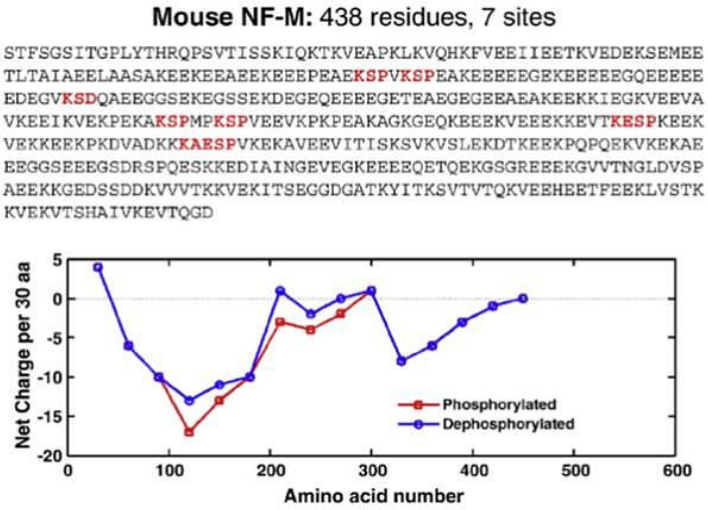


Fig. 5.5. Aminoacid sequence of mouse NFM obtained from Uniprot (Forno et al.). The KSP repeats are highlighted in red color (Top). Net charge calculated for every 30 aa acid residues in phosphorylated and dephosphorylated states. Adapted from Stevenson, W., R. Chang and Y. Gebremichael (2011). "Phosphorylation-mediated conformational changes in the mouse neurofilament architecture: insight from a neurofilament brush model." J Mol Biol 405(4): 1101-1118 with permission from Elseiver.

Due to insufficient equilibration, conclusive evidence could not be obtained towards the intended hypothesis in this study. The data shown here represents the average properties of the structure at ~32 ns. When compared to a similar study on human NFH (606 residues and 51 KSP sites) which stabilized in < 6 ns, arriving at the equilibrium structure for the present system was challenging despite the relatively shorter length and lower number of KSP residues (430 residues and 7 KSP

sites) . The simulations were performed up to 32 ns which is about 5 times the duration required for human NFH equilibration in a previous study (Adiga et al. 2009). The plausible explanation to difficulty in equilibrating the structure is given by examining the sequence distribution of NFM. Figure 5.5 shows the amino acid sequence of the NFM, where the KSP motifs are highlighted in red. Also included is the charge distribution of NFM in the presence and absence of phosphorylation. The charge is calculated per every 30 aa. As seen in the figure 5.5, the NFM structure has evenly distributed negatively charged residues across its length in both phosphorylated states. The aminoacid composition consists of about ~30% Glu (-1e) residues and 17% Lys (+1e) which confers a net negative charge of -64 e. In addition, the KSP motifs are interspersed across the length, and upon phosphorylation add to the existing negative charge (-2e per serine) which also influences the charge distribution of the structure. The stretches of glutamic acid in addition to the KSP residues confer an extended helical structure to NFM. The structure is dominated by electrostatic repulsions between the negatively charged residues in both phosphorylation states. Due to the presence of such high electrostatic interactions, arriving at an equilibrium structure for the present system in both phosphorylation states has proven challenging. Based on the trend observed, equilibration could take approximately 40-50 ns or more of simulation time.

Nevertheless, the trend of these preliminary results suggests that phosphorylation has a minimal effect on the conformational changes in mouse NFM. Upon equilibration, the conformational analysis may provide valuable insights onto the key molecular changes governing the structure. This knowledge can be helpful in comprehending the regulatory mechanism adapted by NFM in mediating the radial growth.

# Chapter VI

## Conclusion & Future directions

*Summary*

In this work, we explored the structural basis of NF organization, particularly the conformational modulations of NF C-terminal domains, by employing computational modelling techniques. Sidearm mediated NF interactions are correlated with the expansion of axonal volume and stability of the axon. Towards specific aim 1, we explored the conformational dynamics of interacting neurofilaments under different phosphorylation and ionic conditions. The studies suggest entropic exclusion as the likely mechanism of sidearm mediated NF interaction under physiological conditions. However, to precisely resolve the mechanism of NF interactions, further investigations on the free energy and entropy of interacting filaments is warranted.

The conformational properties C-terminal domains are sensitive to subtle changes in the intra-cellular environment such as pH, ionic strength, influx of divalent ions. Therefore, towards specific aim 2 we explored the NF brush structure in the presence of varying strengths of $Ca^{2+}$ concentration. NF sidearms have hydrophobic moieties that comprise a significant portion of their length. However, their influence on NF brush structure has not been investigated previously. Therefore, in the present study by including the effect of hydrophobic interactions we also investigated their influence on the NF brush structure. The presence of $Ca^{2+}$ ions induced a reduction in the sidearm dimensions at low ionic strengths (I = 1 mM, 10 mM). However, the effect was minimal at near physiological ionic conditions (I = 100 mM). Although a small contraction in the overall length of the sidearms has been observed, the hydrophobic interactions did not exert significant influence on the NF structure. The study enhanced our understanding on the effects of ionic strength and divalent ion concentration on the conformations of the NF sidearms. These observations in combination with previous studies provide a comprehensive overview of the NF sidearm properties in under varying environmental conditions.

Recent gene targeting studies have implicated NFM as the potential determinant of axonal diameter. Further, it is believed that the NFM mediated axonal expansion is independent of phosphorylation. Towards specific aim 3 we attempted to examine the structural transitions of NFM polypeptide in response to phosphorylation at an atomistic level. The result of this study, though inconclusive at the present stage, does not show a significant difference between phosphorylated and dephosphorylated systems in the mouse NFM structure.

Limitations of the Models

We used two different computational models for the studies presented in this report. 1) 3D Coarse grained model and 2) Atomistic model. The coarse grained 3D model uses a simplified approximation of interactions between the NF core and the sidearm or between the sidearms by the sum of excluded volume, electrostatic, and hydrophobic interactions, where both monovalent salt ions and solvents are implicitly incorporated into the electrostatic interaction potential. Consequently, the limitation of this simplified approximation is that some detailed properties of the system cannot be captured. Due to the implicit treatment of both monovalent ions and salt through interaction potential, solvent specific interactions such as hydrogen bonding cannot be captured. In addition, since the NF backbone is treated as neutral cylindrical rod, the interactions between the filament backbone and the sidearm monomers are accounted only through excluded volume interactions. Possible electrostatic and hydrophobic interactions between the backbone and the sidearms are ignored, which may have some effect on the conformations of NF sidearms, although due to the ionic screening these effects are expected to be minimal under physiological conditions.

Atomistic model was used to study the NFM polypeptide under different phosphorylation conditions. The main challenge in this model is the prolonged structural relaxation of the molecules that makes it computationally expensive and time for systems such as NFM sidearm.

Future Directions

Elucidating the molecular mechanism that maintains the equilibrium of cytoskeletal network is an important part of identifying the pathophysiology relating to NF accumulations in humans. Our research is a step towards providing a theoretical perspective of the structural variations in NF sidearms under different cellular conditions. This knowledge in combination with experimental studies can shed light onto the possible mechanisms underlying the axonal growth process. Our work may have some limitation in capturing the sidearm interactions with the core. Nevertheless, the studies provided descriptive understanding of the conformational dynamics of the NF C-terminal domains under different physiological and non-physiological conditions. It would be interesting to extend the present model to study the compaction of NFs observed in axonal injury in future. Additionally, upon fully equilibration, the atomistic model may provide detailed information on the role of key residues in regulating the lateral extension of NFM sidearms in mouse.

## APPENDIX I

Wild type Mouse NF-M C-terminus (red amino acids were deleted in Δ NFM)

KLLEGEETRFSTFSGSITGPLYTHRQPSVTISSKIQKTKVEAPKLKVQHKFVEEIIEETKVEDEKSEMEETLTAIAEELAASAKE
EKEEAEEKEEEPEAEKSPVKSPEAKEEEEEGEKEEEEEGQEEEEEEDEGVKSDQAEEGGSEKEGSSEKDEGEQEEEEGETE
AEGEGEEAEAKEEKKIEGKVEEVAVKEEIKVEKPEKAKSPMPKSPVEEVKPKPEAKAGKGEXKEEEKVEEEKKEVTKESPK
EEKVEKKEEKPKDVADKKKAESPVKEKAVEEVITISKSXKVSLEKDTKEEKXQPQEKVKEKAEEEGGSEEEGSDRSPQESKK
EDIAINGEVEGKEEEEQETQEKGSGREEEKGVVTNGLDVSPAEEKKGEDSSDDKVVVTKKVEKITSEGGDGATKYITKSV
TVTQKVEEHEETFEEKLVSTKKVEKVTSHAIVKEVTQGD

Mouse NF-MΔ85a.a. C-terminus

KLLEGEEKEEEPEAEKSPVKSPEAKEEEEEGEKEEEEEGQEEEEEEDEGVKSDQAEEGGSEKEGSSEKDEGEQEEEEGETE
AEGEGEEAEAKEEKKIEGKVEEVAVKEEIKVEKPEKAKSPMPKSPVEEVKPKPEAKAGKGEXKEEEKVEEEKKEVTKESPK
EEKVEKKEEKPKDVADKKKAESPVKEKAVEEVITISKSXKVSLEKDTKEEKXQPQEKVKEKAEEEGGSEEEGSDRSPQESKK
EDIAINGEVEGKEEEEQETQEKGSGREEEKGVVTNGLDVSPAEEKKGEDSSDDKVVVTKKVEKITSEGGDGATKYITKSV
TVTQKVEEHEETFEEKLVSTKKVEKVTSHAIVKEVTQGD

**REFERENCES**

Aamodt, E. J. and R. C. Williams, Jr. (1984). "Microtubule-associated proteins connect microtubules and neurofilaments in vitro." Biochemistry **23**(25): 6023-6031.

Ackerley, S., P. Thornhill, A. J. Grierson, J. Brownlees, B. H. Anderton, P. N. Leigh, C. E. Shaw and C. C. Miller (2003). "Neurofilament heavy chain side arm phosphorylation regulates axonal transport of neurofilaments." Journal of Cell Biology **161**(3): 489-495.

Adiga, S.P. Brenner, D.W. "Molecular Basis for Neurofilament Heavy Chain Side Arm Structure Modulation by Phosphorylation". The Journal of Physical Chemistry C 114 (12), 5410-5416

Barry, D. M., S. Millecamps, J. P. Julien and M. L. Garcia (2007). "New movements in neurofilament transport, turnover and disease." Experimental Cell Research **313**(10): 2110-2120.

Barry, D. M., W. Stevenson, B. G. Bober, P. J. Wiese, J. M. Dale, G. S. Barry, N. S. Byers, J. D. Strope, R. Chang, D. J. Schulz, S. Shah, N. A. Calcutt, Y. Gebremichael and M. L. Garcia (2012). "Expansion of neurofilament medium C terminus increases axonal diameter independent of increases in conduction velocity or myelin thickness." Journal of Neuroscience **32**(18): 6209-6219.

Beck, R., J. Deek, J. B. Jones and C. R. Safinya (2010). "Gel-expanded to gel-condensed transition in neurofilament networks revealed by direct force measurements." Nat Mater **9**(1): 40-46.

Beck, R., J. Deek and C. R. Safinya (2012). "Structures and interactions in 'bottlebrush' neurofilaments: the role of charged disordered proteins in forming hydrogel networks." Biochemical Society Transactions **40**: 1027-1031.

Brown, A. (2000). "Slow axonal transport: stop and go traffic in the axon." Nat Rev Mol Cell Biol **1**(2): 153-156.

Brown, H. G. and J. H. Hoh (1997). "Entropic exclusion by neurofilament sidearms: A mechanism for maintaining interfilament spacing." Biochemistry **36**(49): 15035-15040.

Buki, A. and J. T. Povlishock (2006). "All roads lead to disconnection?--Traumatic axonal injury revisited." Acta Neurochir (Wien) **148**(2): 181-193; discussion 193-184.

Carden, M. J., J. Q. Trojanowski, W. W. Schlaepfer and V. M. Lee (1987). "Two-stage expression of neurofilament polypeptides during rat neurogenesis with early establishment of adult phosphorylation patterns." J. Neurosci. **7**(11): 3489-3504.

Carpenter, D. A. and W. Ip (1996). "Neurofilament protein interactions: Evidence for the preferred formation NF-L-containing dimers and a putative function for the end domains." Journal of Cell Science **109**: 2493-2498.

Carter, J., A. Gragerov, K. Konvicka, G. Elder, H. Weinstein and R. A. Lazzarini (1998). "Neurofilament (NF) assembly; Divergent characteristics of human and rodent NF-L subunits." Journal of Biological Chemistry **273**(9): 5101-5108.

Chang, R., Y. Kwak and Y. Gebremichael (2009). "Structural properties of neurofilament sidearms: sequence-based modeling of neurofilament architecture." J Mol Biol **391**(3): 648-660.

Chang, R. W. and A. Yethiraj (2003). "Brownian dynamics simulations of polyelectrolyte solutions with divalent counterions." Journal of Chemical Physics **118**(24): 11315-11325.

Chen, J. H., W. P. Im and C. L. Brooks (2006). "Balancing solvation and intramolecular interactions: Toward a consistent generalized born force field." J Am Chem Soc **128**(11): 3728-3736.

Cherstvy, A. G. and Winkler, R. G.(2011). " Polyelectrolyte adsorption onto oppositely charged interfaces: unified approach for plane, cylinder, and sphere". Phys Chem Chem Phys **13**(24): 11686-93

Chervanyov, A. I.and Heinrich, G.(2009)." Potential theory of the depletion interaction in the colloid-polymer mixtures".J Chem Phys 131(23): 234907

Craciun, G., A. Brown and A. Friedman (2005). "A dynamical system model of neurofilament transport in axons." J Theor Biol **237**(3): 316-322.

Dashiell, S. M., S. L. Tanner, H. C. Pant and R. H. Quarles (2002). "Myelin-associated glycoprotein modulates expression and phosphorylation of neuronal cytoskeletal elements and their associated kinases." Journal of Neurochemistry **81**(6): 1263-1272.

de Waegh, S. M., V. M. Lee and S. T. Brady (1992). "Local modulation of neurofilament phosphorylation, axonal caliber, and slow axonal transport by myelinating Schwann cells." Cell **68**(3): 451-463.

Dubois, E. and F. Boue (2001). "Conformation of poly(styrenesulfonate) polyions in the presence of multivalent ions: Small-angle neutron scattering experiments." Macromolecules **34**(11): 3684-3697.

Elder, G. A., V. L. Friedrich, Jr., P. Bosco, C. Kang, A. Gourov, P. H. Tu, V. M. Lee and R. A. Lazzarini (1998). "Absence of the mid-sized neurofilament subunit decreases axonal calibers, levels of light neurofilament (NF-L), and neurofilament content." Journal of Cell Biology **141**(3): 727-739.

Elder, G. A., V. L. Friedrich, Jr., C. Kang, P. Bosco, A. Gourov, P. H. Tu, B. Zhang, V. M. Lee and R. A. Lazzarini (1998). "Requirement of heavy neurofilament subunit in the development of axons with large calibers." Journal of Cell Biology **143**(1): 195-205.

Elder, G. A., V. L. Friedrich, Jr., A. Margita and R. A. Lazzarini (1999). "Age-related atrophy of motor axons in mice deficient in the mid-sized neurofilament subunit." Journal of Cell Biology **146**(1): 181-192.

Elder, G. A., V. L. Friedrich, Jr., D. Pereira, P. H. Tu, B. Zhang, V. M. Lee and R. A. Lazzarini (1999). "Mice with disrupted midsized and heavy neurofilament genes lack axonal neurofilaments but have unaltered numbers of axonal microtubules." J Neurosci Res **57**(1): 23-32.

Fliegner, K. H. and R. K. Liem (1991). "Cellular and molecular biology of neuronal intermediate filaments." Int Rev Cytol **131**: 109-167.

Forno, L. S., L. A. Sternberger, N. H. Sternberger, A. M. Strefling, K. Swanson and L. F. Eng (1986). "Reaction of Lewy Bodies with Antibodies to Phosphorylated and Nonphosphorylated Neurofilaments." Neuroscience Letters **64**(3): 253-258.

Friede, R. L. and T. Samorajski (1970). "Axon caliber related to neurofilaments and microtubules in sciatic nerve fibers of rats and mice." Anatomical Record **167**(4): 379-387.

Frishchknecht, A. L. (2008). "Forces between nanorods with end-adsorbed chains in a homopolymer melt." J. Chem. Phys. **128**(224902).

Fuchs, E. and D. W. Cleveland (1998). "A structural scaffolding of intermediate filaments in health and disease." Science **279**(5350): 514-519.

Garcia, M. L., C. S. Lobsiger, S. B. Shah, T. J. Deerinck, J. Crum, D. Young, C. M. Ward, T. O. Crawford, T. Gotow, Y. Uchiyama, M. H. Ellisman, N. A. Calcutt and D. W. Cleveland (2003). "NF-M is an essential target for the myelin-directed "outside-in" signaling cascade that mediates radial axonal growth." Journal of Cell Biology **163**(5): 1011-1020.

Garcia, M. L., M. V. Rao, J. Fujimoto, V. B. Garcia, S. B. Shah, J. Crum, T. Gotow, Y. Uchiyama, M. Ellisman, N. A. Calcutt and D. W. Cleveland (2009). "Phosphorylation of highly conserved neurofilament medium KSP repeats is not required for myelin-dependent radial axonal growth." Journal of Neuroscience **29**(5): 1277-1284.

Gill, S. R., P. C. Wong, M. J. Monteiro and D. W. Cleveland (1990). "Assembly properties of dominant and recessive mutations in the small mouse neurofilament (NF-L) subunit." Journal of Cell Biology **111**(5 Pt 1): 2005-2019.

Glicksman, M. A., D. Soppet and M. B. Willard (1987). "Posttranslational modification of neurofilament polypeptides in rabbit retina." J. Neurobiol. **18**(2): 167-196.

Gong, C. X., S. Shaikh, J. Z. Wang, T. Zaidi, I. Grundkeiqbal and K. Iqbal (1995). "Phosphatase-Activity toward Abnormally Phosphorylated-Tau - Decrease in Alzheimer-Disease Brain." Journal of Neurochemistry **65**(2): 732-738.

Gong, C. X., T. J. Singh, I. Grundkeiqbal and K. Iqbal (1993). "Phosphoprotein Phosphatase-Activities in Alzheimer-Disease Brain." Journal of Neurochemistry **61**(3): 921-927.

Gou, J. P., T. Gotow, P. A. Janmey and J. F. Leterrier (1998). "Regulation of neurofilament interactions in vitro by natural and synthetic polypeptides sharing Lys-Ser-Pro sequences with the heavy neurofilament subunit NF-H: Neurofilament crossbridging by antiparallel sidearm overlapping." Medical & Biological Engineering & Computing **36**(3): 371-387.

Grant, P. and H. C. Pant (2000). "Neurofilament protein synthesis and phosphorylation." Journal of Neurocytology **29**(11-12): 843-872.

Heins, S., P. C. Wong, S. Muller, K. Goldie, D. W. Cleveland and U. Aebi (1993). "The rod domain of NF-L determines neurofilament architecture, whereas the end domains specify filament assembly and network formation." Journal of Cell Biology **123**(6 Pt 1): 1517-1533.

Herrmann H, Aebi U. Intermediate filaments: molecular structure, assembly mechanism, and integration into functionally distinct intracellular scaffolds. Annual Review of Biochemistry. 2004;73:749–89

Hirokawa, N. (1982). "Cross-linker system between neurofilaments, microtubules, and membranous organelles in frog axons revealed by the quick-freeze, deep-etching method." Journal of Cell Biology **94**(1): 129-142.

Hirokawa, N. (1982). "Cross-Linker system between Neurofilaments, Microtubules, and membranous organelles in frog axons revealed by the Quick-Freeze, deep-etching method." Journal of Cell Biology **94**(1): 129-142.

Hirokawa, N., M. A. Glicksman and M. B. Willard (1984). "Organization of Mammalian Neurofilament Polypeptides within the Neuronal Cytoskeleton." Journal of Cell Biology **98**(4): 1523-1536.

Hirokawa, N., S. Hisanaga and Y. Shiomura (1988). "MAP2 is a component of crossbridges between microtubules and neurofilaments in the neuronal cytoskeleton: quick-freeze, deep-etch immunoelectron microscopy and reconstitution studies." Journal of Neuroscience **8**(8): 2769-2779.

Hisanaga, S., Y. Gonda, M. Inagaki, A. Ikai and N. Hirokawa (1990). "Effects of Phosphorylation of the Neurofilament L-Protein on Filamentous Structures." Cell Regulation **1**(2): 237-248.

Hodes, R. (1953). "Linear Relationship between Fiber Diameter and Velocity of Conduction in Giant Axon of Squid." Journal of Neurophysiology **16**(2): 145-154.

Hoffman, P. N., R. J. Lasek, J. W. Griffin and D. L. Price (1983). "Slowing of the axonal transport of neurofilament proteins during development." Journal of Neuroscience **3**(8): 1694-1700.

Howell, W. H., J. F. Fulton, T. C. Ruch and H. D. Patton (1973). Physiology and biophysics. Philadelphia, Saunders.

Hsieh, S. T., T. O. Crawford and J. W. Griffin (1994). "Neurofilament Distribution and Organization in the Myelinated Axons of the Peripheral Nervous-System." Brain Research **642**(1-2): 316-326.

Hsieh, S. T., G. J. Kidd, T. O. Crawford, Z. S. Xu, W. M. Lin, B. D. Trapp, D. W. Cleveland and J. W. Griffin (1994). "Regional Modulation of Neurofilament Organization by Myelination in Normal Axons." J. Neurosci. **14**(11): 6392-6401.

Im, W. P., M. S. Lee and C. L. Brooks (2003). "Generalized born model with a simple smoothing function." Journal of Computational Chemistry **24**(14): 1691-1702.

Jacomy, H., Q. Zhu, S. Couillard-Despres, J. M. Beaulieu and J. P. Julien (1999). "Disruption of type IV intermediate filament network in mice lacking the neurofilament medium and heavy subunits." Journal of Neurochemistry **73**(3): 972-984.

Janmey, P. A., J. F. Leterrier and H. Herrmann (2003). "Assembly and structure of neurofilaments." Current Opinion in Colloid & Interface Science **8**(1): 40-47.

Jayanthi, L., W. Stevenson, Y. Kwak, R. Chang and Y. Gebremichael (2013). "Conformational properties of interacting neurofilaments: Monte Carlo simulations of cylindrically grafted apposing neurofilament brushes." J Biol Phys **39**(3): 343-362.

Jones, M. R., C. Liu and A. K. Wilson (2014). "Molecular dynamics studies of the protein-protein interactions in inhibitor of kappaB kinase-beta." J Chem Inf Model **54**(2): 562-572.

Jung, C., J. T. Yabe and T. B. Shea (2000). "C-terminal phosphorylation of the high molecular weight neurofilament subunit correlates with decreased neurofilament axonal transport velocity." Brain Research **856**(1-2): 12-19.

Kerrigan, J. E. (2013). "Molecular dynamics simulations in drug design." Methods Mol Biol **993**: 95-113.

Kim, S., R. Chang, C. Teunissen, Y. Gebremichael and A. Petzold (2011). "Neurofilament stoichiometry simulations during neurodegeneration suggest a remarkable self-sufficient and stable in vivo protein structure." J Neurol Sci **307**(1-2): 132-138.

Korobko, A. V., W. Jesse, S. U. Egelhaaf, A. Lapp and J. R. van der Maarel (2004). "Do spherical polyelectrolyte brushes interdigitate?" Phys Rev Lett **93**(17): 177801.

Korobko, A. V., W. Jesse, S. U. Egelhaaf, A. Lapp and J. R. van der Maarel (2004). "Do spherical polyelectrolyte brushes interdigitate?" Phys. Rev. Lett. **93**(17): 177801.

Kreplak, L., H. Bar, J. F. Leterrier, H. Herrmann and U. Aebi (2005). "Exploring the mechanical behavior of single intermediate filaments." J Mol Biol **354**(3): 569-577.

Kriz, J., Q. Z. Zhu, J. P. Julien and A. L. Padjen (2000). "Electrophysiological properties of axons in mice lacking neurofilament subunit genes: disparity between conduction velocity and axon diameter in absence of NF-H." Brain Research **885**(1): 32-44.

Kumar, S. and J. H. Hoh (2004). "Modulation of repulsive forces between neurofilaments by sidearm phosphorylation." Biochemical and Biophysical Research Communications **324**(2): 489-496.

Kumar, S., X. Yin, B. D. Trapp, J. H. Hoh and M. E. Paulaitis (2002). "Relating interactions between neurofilaments to the structure of axonal neurofilament distributions through polymer brush models." Biophys J **82**(5): 2360-2372.

Kushkuley, J., S. Metkar, W. K. H. Chan, S. Lee and T. B. Shea (2010). "Aluminum induces neurofilament aggregation by stabilizing cross-bridging of phosphorylated c-terminal sidearms." Brain Research **1322**: 118-123.

Lasek, R. J., P. Paggi and M. J. Katz (1992). "Slow axonal transport mechanisms move neurofilaments relentlessly in mouse optic axons." Journal of Cell Biology **117**(3): 607-616.

Lee, J., S. Kim, R. Chang, L. Jayanthi and Y. Gebremichael (2013). "Effects of molecular model, ionic strength, divalent ions, and hydrophobic interaction on human neurofilament conformation." J Chem Phys **138**(1): 015103.

Lee, M. K., & Cleveland, D. W. (1996). Neuronal intermediate filaments. Annual review of neuroscience, **19**(1), 187-217.

Lee, M. K., J. R. Marszalek and D. W. Cleveland (1994). "A Mutant Neurofilament Subunit Causes Massive, Selective Motor-Neuron Death - Implications for the Pathogenesis of Human Motor-Neuron Disease." Neuron **13**(4): 975-988.

Leterrier, J. F., J. Kas, J. Hartwig, R. Vegners and P. A. Janmey (1996). "Mechanical effects of neurofilament cross-bridges - Modulation by phosphorylation, lipids, and interactions with F-actin." Journal of Biological Chemistry **271**(26): 15687-15694.

Leterrier, J. F., R. K. Liem and M. L. Shelanski (1982). "Interactions between neurofilaments and microtubule-associated proteins: a possible mechanism for intraorganellar bridging." Journal of Cell Biology **95**(3): 982-986.

Letterier, J. F., and Eyre, J (1987). "Properties of highly viscous gels formed by neurofilament in vitro: A possible consequence of a specific inter-filament cross-bridging." Biochem. J. **245**: 93-101.

Lewis, S. E. and R. A. Nixon (1988). "Multiple phosphorylated variants of the high molecular mass subunit of neurofilaments in axons of retinal cell neurons: characterization and evidence for their differential association with stationary and moving neurofilaments." Journal of Cell Biology **107**(6 Pt 2): 2689-2701.

Lin, Y. C., N. Y. Yao, C. P. Broedersz, H. Herrmann, F. C. Mackintosh and D. A. Weitz (2010). "Origins of elasticity in intermediate filament networks." Phys Rev Lett **104**(5): 058101.

Liu, J., X. J. Tong, S. J. Pang and Z. H. Zhai (1999). "The periodicity in the structure of native neurofilaments studied with scanning tunneling microscopy." Applied Surface Science **144-45**: 644-647.

Lyons, A. J., N. S. Gandhi and R. L. Mancera (2014). "Molecular dynamics simulation of the phosphorylation-induced conformational changes of a tau peptide fragment." Proteins.

Manetto, V., N. H. Sternberger, G. Perry, L. A. Sternberger and P. Gambetti (1988). "Phosphorylation of Neurofilaments Is Altered in Amyotrophic Lateral Sclerosis." Journal of Neuropathology and Experimental Neurology **47**(6): 642-653.

Marszalek, J. R., T. L. Williamson, M. K. Lee, Z. S. Xu, P. N. Hoffman, M. W. Becher, T. O. Crawford and D. W. Cleveland (1996). "Neurofilament subunit NF-H modulates axonal diameter by selectively slowing neurofilament transport." Journal of Cell Biology **135**(3): 711-724.

Martin, R., R. Door, A. Ziegler, W. Warchol, J. Hahn and D. Breitig (1999). "Neurofilament phosphorylation and axon diameter in the squid giant fibre system." Neuroscience **88**(1): 327-336.

Mata, M., N. Kupina and D. J. Fink (1992). "Phosphorylation-Dependent Neurofilament Epitopes Are Reduced at the Node of Ranvier." Journal of Neurocytology **21**(3): 199-210.

McHale, M. K., G. F. Hall and M. J. Cohen (1995). "Early cytoskeletal changes following injury of giant spinal axons in the lamprey." J Comp Neurol **353**(1): 25-37.

McQuarrie, D. A. (2000). Statistical mechanics. Sausalito, Calif., University Science Books.

Monteiro, M. J., P. N. Hoffman, J. D. Gearhart and D. W. Cleveland (1990). "Expression of Nf-L in Both Neuronal and Nonneuronal Cells of Transgenic Mice - Increased Neurofilament Density in Axons without Affecting Caliber." Journal of Cell Biology **111**(4): 1543-1557.

Morris, J. R. and R. J. Lasek (1982). "Stable Polymers of the Axonal Cytoskeleton - the Axoplasmic Ghost." Journal of Cell Biology **92**(1): 192-198.

Mukhopadhyay, R., S. Kumar and J. H. Hoh (2004). "Molecular mechanisms for organizing the neuronal cytoskeleton." Bioessays **26**(9): 1017-1025.

Muma, N. A., H. H. Slunt and P. N. Hoffman (1991). "Postnatal Increases in Neurofilament Gene-Expression Correlate with the Radial Growth of Axons." Journal of Neurocytology **20**(10): 844-854.

Nixon, R. A. (1998). "The slow axonal transport of cytoskeletal proteins." Current Opinion in Cell Biology **10**(1): 87-92.

Nixon, R. A., P. A. Paskevich, R. K. Sihag and C. Y. Thayer (1994). "Phosphorylation on Carboxyl-Terminus Domains of Neurofilament Proteins in Retinal Ganglion-Cell Neurons in-Vivo - Influences on Regional Neurofilament Accumulation, Interneurofilament Spacing, and Axon Caliber." Journal of Cell Biology **126**(4): 1031-1046.

Nixon, R. A. and T. B. Shea (1992). "Dynamics of Neuronal Intermediate Filaments - a Developmental Perspective." Cell Motility and the Cytoskeleton **22**(2): 81-91.

Ohara, O., Y. Gahara, T. Miyake, H. Teraoka and T. Kitamura (1993). "Neurofilament Deficiency in Quail Caused by Nonsense Mutation in Neurofilament-L Gene." Journal of Cell Biology **121**(2): 387-395.

Okonkwo, D. O., E. H. Pettus, J. Moroi and J. T. Povlishock (1998). "Alteration of the neurofilament sidearm and its relation to neurofilament compaction occurring with traumatic axonal injury." Brain Research **784**(1-2): 1-6.

Pant, H. C. (1988). "Dephosphorylation of neurofilament proteins enhances their susceptibility to degradation by calpain." Biochemical Journal **256**(2): 665-668.

Panwar, A. S. and S. Kumar (2005). "Brownian dynamics simulations of polyelectrolyte adsorption in shear flow." J. Chem. Phys. **122**(15): 154902.

Pappolla, M. A. (1986). "Lewy Bodies of Parkinsons-Disease - Immune Electron-Microscopic Demonstration of Neurofilament Antigens in Constituent Filaments." Archives of Pathology & Laboratory Medicine **110**(12): 1160-1163.

Perrot, R., R. Berges, A. Bocquet and J. Eyer (2008). "Review of the multiple aspects of neurofilament functions, and their possible contribution to neurodegeneration." Mol Neurobiol **38**(1): 27-65.

Perrot, R. and J. Eyer (2009). "Neuronal intermediate filaments and neurodegenerative disorders." Brain Research Bulletin **80**(4-5): 282-295.

Perrot, R., P. Lonchampt, A. C. Peterson and J. Eyer (2007). "Axonal neurofilaments control multiple fiber properties but do not influence structure or spacing of nodes of Ranvier." Journal of Neuroscience **27**(36): 9573-9584.

Petzold, A., D. Gveric, M. Groves, K. Schmierer, D. Grant, M. Chapman, G. Keir, L. Cuzner and E. J. Thompson (2008). "Phosphorylation and compactness of neurofilaments in multiple sclerosis: Indicators of axonal pathology." Exp Neurol **213**(2): 326-335.

Povlishock, J. T. and C. W. Christman (1995). "The pathobiology of traumatically induced axonal injury in animals and humans: a review of current thoughts." J Neurotrauma **12**(4): 555-564.

Price, R. L., P. Paggi, R. J. Lasek and M. J. Katz (1988). "Neurofilaments are spaced randomly in the radial dimension of axons." Journal of Neurocytology **17**(1): 55-62.

Price, R. L., P. Paggi, R. J. Lasek and M. J. Katz (1988). "Neurofilaments are spaced randomly in the radial dimension of axons." Journal of Neurocytology **17**(1): 55-62.

Qianqian cao, C. Z., Hongwei He, Lujuan Li (2009). "A molecular dynamics study of two apposing polyelectrolyte brushes with mono and multivalent counterions." Macromol. Theory Simul. **18**: 441-452.

Rammensee, S., Janmey, P.A., Bausch, A.R. (2007). " Mechanical and structural properties of in vitro neurofilament hydrogels." European Biophysics Journal **36**: 661-668

Rao, M. V., J. Campbell, A. D. Yuan, A. Kumar, T. Gotow, Y. Uchiyama and R. A. Nixon (2003). "The neurofilament middle molecular mass subunit carboxyl-terminal tail domains is essential for the radial growth and cytoskeletal architecture of axons but not for regulating neurofilament transport rate." Journal of Cell Biology **163**(5): 1021-1031.

Rao, M. V., M. L. Garcia, Y. Miyazaki, T. Gotow, A. D. Yuan, S. Mattina, C. M. Ward, N. A. Calcutt, Y. Uchiyama, R. A. Nixon and D. W. Cleveland (2002). "Gene replacement in mice reveals that the heavily phosphorylated tail of neurofilament heavy subunit does not affect axonal caliber or the transit of cargoes in slow axonal transport." Journal of Cell Biology **158**(4): 681-693.

Rao, M. V., M. K. Houseweart, T. L. Williamson, T. O. Crawford, J. Folmer and D. W. Cleveland (1998). "Neurofilament-dependent radial growth of motor axons and axonal organization of neurofilaments does not require the neurofilament heavy subunit (NF-H) or its phosphorylation." Journal of Cell Biology **143**(1): 171-181.

Rao, M. V., M. K. Houseweart, T. L. Williamson, T. O. Crawford, J. Folmer and D. W. Cleveland (1998). "Neurofilament-dependent radial growth of motor axons and axonal organization of neurofilaments does not require the neurofilament heavy subunit (NF-H) or its phosphorylation." Journal of Cell Biology **143**(1): 171-181.

Reles, A. and R. L. Friede (1991). "Axonal Cytoskeleton at the Nodes of Ranvier." Journal of Neurocytology **20**(6): 450-458.

Roy, S., P. Coffee, G. Smith, R. K. Liem, S. T. Brady and M. M. Black (2000). "Neurofilaments are transported rapidly but intermittently in axons: implications for slow axonal transport." Journal of Neuroscience **20**(18): 6849-6861.

Sakaguchi, T., M. Okada, T. Kitamura and K. Kawasaki (1993). "Reduced Diameter and Conduction-Velocity of Myelinated Fibers in the Sciatic-Nerve of a Neurofilament-Deficient Mutant Quail." Neuroscience Letters **153**(1): 65-68.

Sanchez, I., L. Hassinger, R. K. Sihag, D. W. Cleveland, P. Mohan and R. A. Nixon (2000). "Local control of neurofilament accumulation during radial growth of myelinating axons in vivo: Selective role of site-specific phosphorylation." Journal of Cell Biology **151**(5): 1013-1024.

Scheraga, H. A., M. Khalili and A. Liwo (2007). "Protein-folding dynamics: overview of molecular simulation techniques." Annu Rev Phys Chem **58**: 57-83.

Shah, J. V. and D. W. Cleveland (2002). "Slow axonal transport: fast motors in the slow lane." Current Opinion in Cell Biology **14**(1): 58-62.

Shetty, K. T., W. T. Link and H. C. Pant (1993). "cdc2-like kinase from rat spinal cord specifically phosphorylates KSPXK motifs in neurofilament proteins: isolation and characterization." Proc Natl Acad Sci U S A **90**(14): 6844-6848.

Sihag, R. K., H. Jaffe, R. A. Nixon and X. H. Rong (1999). "Serine-23 is a major protein kinase A phosphorylation site on the amino-terminal head domain of the middle molecular mass subunit of neurofilament proteins." Journal of Neurochemistry **72**(2): 491-499.

Sihag, R. K. and R. A. Nixon (1989). "Invivo Phosphorylation of Distinct Domains of the 70-Kilodalton Neurofilament Subunit Involves Different Protein-Kinases." Journal of Biological Chemistry **264**(1): 457-464.

Sihag, R. K. and R. A. Nixon (1991). "Identification of Ser-55 as a Major Protein Kinase-a Phosphorylation Site on the 70-Kda Subunit of Neurofilaments - Early Turnover during Axonal-Transport." Journal of Biological Chemistry **266**(28): 18861-18867.

Smit, D. F. a. B. (2002). Understanding Molecular Simulation: From Algorithms to Applications Academic Press.

Smit., D. F. B. (2002). Understanding molecular simulation. San Diego, CA, Academic Press.

Smith, D. H., K. Uryu, K. E. Saatman, J. Q. Trojanowski and T. K. McIntosh (2003). "Protein accumulation in traumatic brain injury." Neuromolecular Med **4**(1-2): 59-72.

Steinert, P. M. and D. R. Roop (1988). "Molecular and cellular biology of intermediate filaments." Annu Rev Biochem **57**: 593-625.

Stevens, M. J. and J. H. Hoh (2010). "Conformational dynamics of neurofilament side-arms." J Phys Chem B **114**(27): 8879-8886.

Stevens, M. J. and J. H. Hoh (2011). "Interactions between Planar Grafted Neurofilament Side-Arms." J. Phys. Chem. B **115**(23): 7541-7549.

Stevenson, W., R. Chang and Y. Gebremichael (2011). "Phosphorylation-mediated conformational changes in the mouse neurofilament architecture: insight from a neurofilament brush model." J Mol Biol **405**(4): 1101-1118.

Terada, S., T. Nakata, A. C. Peterson and N. Hirokawa (1996). "Visualization of slow axonal transport in vivo." Science **273**(5276): 784-788.

Veeranna, D. S. Yang, J. H. Lee, K. Y. Vinod, P. Stavrides, N. D. Amin, H. C. Pant and R. A. Nixon (2011). "Declining phosphatases underlie aging-related hyperphosphorylation of neurofilaments." Neurobiology of Aging **32**(11): 2016-2029.

Vogel, P., M. Gabriel, H. H. Goebel and P. J. Dyck (1985). "Hereditary Motor Sensory Neuropathy Type-Ii with Neurofilament Accumulation - New Finding or New Disorder." Annals of Neurology **17**(5): 455-461.

Wagner, O. I., Rammensee, S., Korde, N., Wen, Q., Leterrier, J. F., & Janmey, P. A. (2007). Softness, strength and self-repair in intermediate filament networks. Experimental cell research, **313**(10), 2228-2235.

Wang, H. T., M. F. Wu, C. J. Zhan, E. Y. Ma, M. G. Yang, X. Y. Yang and Y. P. Li (2012). "Neurofilament proteins in axonal regeneration and neurodegenerative diseases." Neural Regeneration Research **7**(8): 620-626.

Wang, L. and A. Brown (2001). "Rapid intermittent movement of tubulin in axons." Molecular Biology of the Cell **12**: 182a-182a.

Wang, L., C. L. Ho, D. Sun, R. K. Liem and A. Brown (2000). "Rapid movement of axonal neurofilaments interrupted by prolonged pauses." Nature Cell Biology **2**(3): 137-141.

Wang, L., C. L. Ho, D. M. Sun, R. K. H. Liem and A. Brown (2000). "Rapid movement of axonal neurofilaments interrupted by prolonged pauses." Nature Cell Biology **2**(3): 137-141.

Wittemann, A., M. Drechsler, Y. Talmon and M. Ballauff (2005). "High elongation of polyelectrolyte chains in the osmotic limit of spherical polyelectrolyte brushes: a study by cryogenic transmission electron microscopy." J Am Chem Soc **127**(27): 9688-9689.

Wootton, J. C. and S. Federhen (1996). "Analysis of compositionally biased regions in sequence databases." Computer Methods for Macromolecular Sequence Analysis **266**: 554-571.

Xu, Z., J. R. Marszalek, M. K. Lee, P. C. Wong, J. Folmer, T. O. Crawford, S. T. Hsieh, J. W. Griffin and D. W. Cleveland (1996). "Subunit composition of neurofilaments specifies axonal diameter." Journal of Cell Biology **133**(5): 1061-1069.

Yabe, J. T., C. W. Jung, W. K. H. Chan and T. B. Shea (2000). "Phospho-dependent association of neurofilament proteins with kinesin in situ." Cell Motility and the Cytoskeleton **45**(4): 249-262.

Yan, Y. P. and A. Brown (2005). "Neurofilament polymer transport in axons." Journal of Neuroscience **25**(30): 7014-7021.

Yates, D. M., C. Manser, K. J. De Vos, C. E. Shaw, D. M. McLoughlin and C. C. Miller (2009). "Neurofilament subunit (NFL) head domain phosphorylation regulates axonal transport of neurofilaments." Eur J Cell Biol **88**(4): 193-202.

Yuan, A., R. A. Nixon and M. V. Rao (2006). "Deleting the phosphorylated tail domain of the neurofilament heavy subunit does not alter neurofilament transport rate in vivo." Neuroscience Letters **393**(2-3): 264-268.

Yuan, A., M. V. Rao, A. Kumar, J. P. Julien and R. A. Nixon (2003). "Neurofilament transport in vivo minimally requires hetero-oligomer formation." Journal of Neuroscience **23**(28): 9452-9458.

Yuan, A. D., M. V. Rao, Veeranna and R. A. Nixon (2012). "Neurofilaments at a glance." Journal of Cell Science **125**(14): 3257-3263.

Yuan, A. D., T. Sasaki, M. V. Rao, A. Kumar, V. Kanumuri, D. S. Dunlop, R. K. Liem and R. A. Nixon (2009). "Neurofilaments Form a Highly Stable Stationary Cytoskeleton after Reaching a Critical Level in Axons." Journal of Neuroscience **29**(36): 11316-11329.

Zhang, Y. B., J. F. Douglas, B. D. Ermi and E. J. Amis (2001). "Influence of counterion valency on the scattering properties of highly charged polyelectrolyte solutions." Journal of Chemical Physics **114**(7): 3299-3313.

Zhu, Q., S. Couillard-Despres and J. P. Julien (1997). "Delayed maturation of regenerating myelinated axons in mice lacking neurofilaments." Exp Neurol **148**(1): 299-316.

Zhu, Q. Z., M. Lindenbaum, F. Levavasseur, H. Jacomy and J. P. Julien (1998). "Disruption of the NF-H gene increases axonal microtubule content and velocity of neurofilament transport: Relief of axonopathy resulting from the toxin beta,beta '-iminodipropionitrile." Journal of Cell Biology **143**(1): 183-193.

Zhulina, E. B. and F. A. Leermakers (2007). "A self-consistent field analysis of the neurofilament brush with amino-acid resolution." Biophys J **93**(5): 1421-1430.

**ABSTRACT**

**COMPUTATIONAL INVESTIGATION ON THE STRUCTURAL PROPERTIES OF NEUROFILAMENTS AND THEIR SIDEARMS**

**by**

**LAKSHMI JAYANTHI**

**August 2014**

**Advisor:** Dr. Yeshitila Gebremichael

**Major:** Biomedical Engineering

**Degree:** Doctor of Philosophy

Neurofilaments (NFs) are class IV intermediate filaments, abundantly found in the large diameter myelinated axons. They are the key determinants of axonal diameter and consequently the nerve conduction properties. On the other hand, abnormal NF accumulation has been the hallmark of debilitating neurodegenerative disorders. NF compaction is also one of the pathological manifestations of traumatic axonal injury. However, the exact relation between the disorganized NFs and the etiology of the neurodegenerative disorders is yet to be fully understood. NFs are assembled from three subunits: Low (NFL), Medium (NFM) and Heavy (NFH). These subunits are characterized by a common alpha helical rod domain and carboxyl terminal domains of different lengths specific to each subunit. The tails project from the core of the filament and contain a number of KSP repeat motifs that belongs to the sites for phosphorylation. Especially, the C-terminal tails of NFM and NFH that have relatively longer lengths and higher number of KSP repeats were found to be the key participants of the sidearm-mediated interfilament interactions that regulate the axonal diameter. Though it has been established that the NFs play a central role in determining the axonal caliber, there are several unresolved questions about the structure and functions of NFs.

The overarching goal of our research has been to understand the structural biophysical basis of NF organization. Multi-scale computational models that incorporate electro-physiological characteristics of NFs have been instrumental in revealing these behaviors. The primary objective of my research was to investigate the conformational properties of interacting neurofilaments sidearms using sequence based coarse grained model. This study provided insights into the nature of sidearm mediated NF-NF interaction that determine the axonal caliber. The second objective was to study the structure of an isolated NF model under the influence of hydrophobic interactions and the presence of divalent ions like $Ca^{2+}$. The results enhanced the current understanding of the equilibrium structural properties of the single neurofilament brush system and the effect of cellular changes including ionic strength and presence of divalent ions. The final part objective of our study was to investigate the structural transitions in the mouse NF medium (NFM) subunit at an atomistic level, under the influence of varying physiological parameters. Though conclusive evidence about the key molecular changes underlying the sidearm expansion could not be gathered, the structures exhibit minimal difference with respect to phosphorylation. Overall, the studies provided insightful details of NF architecture up to molecular level, which is essential to elucidate their behavior observed in certain pathological conditions leading to their accumulation and neurodegeneration.

## AUTOBIOGRAPHICAL STATEMENT

Education

PhD in Biomedical Engineering – Aug 2010 –Present
Wayne State University, Detroit, MI
Expected Date of Graduation – Aug 2014

M.Sc in Biomedical Engineering – Jan 2006 – April 2008
Wayne State University, Detroit, MI

B.E. in Biomedical Engineering – Sep 1998 – May 2002
Osmania University, Hyderabad, India

Publications

1. Jayanthi, L., W. Stevenson, Y. Kwak, R. Chang and Y. Gebremichael (2013). "Conformational properties of interacting neurofilaments: Monte Carlo simulations of cylindrically grafted apposing neurofilament brushes." Journal of Biological Physics 39(3): 343-362.
2. Bhatti, G., Jayanthi, L., VandeVord, P., and Gebremichael, Y. (2013). "Computational investigation of the key factors affecting the second stage activation mechanisms of domain II m-calpain. Journal of molecular modeling", 19(2), 779-792.
3. Lee, J., S. Kim, R. Chang, L. Jayanthi and Y. Gebremichael (2013). "Effects of molecular model, ionic strength, divalent ions, and hydrophobic interaction on human neurofilament conformation." Journal of Chemical Physics 138(1): 015103.
4. Computational investigation of the mechanism behind sidearm mediated neurfilament interaction. Poster presentation at The 55th annual Annual Biophysical society meeting at Baltimore, MD, USA in March 2012.
5. Computational investigation of mechanism behind sidearm-mediated neurofilament interaction. Poster presentation at Annual BME research day, Nov 2011, Detroit, USA